

A Class of Models for Large Zero-inflated Spatial Data

Ben Seiyon Lee*

Department of Statistics, George Mason University

Murali Haran

Department of Statistics, The Pennsylvania State University

Abstract

Spatially correlated data with an excess of zeros, usually referred to as zero-inflated spatial data, arise in many disciplines. Examples include count data, for instance, abundance (or lack thereof) of animal species and disease counts, as well as semi-continuous data like observed precipitation. Spatial two-part models are a flexible class of models for such data. Fitting two-part models can be computationally expensive for large data due to high-dimensional dependent latent variables, costly matrix operations, and slow mixing Markov chains. We describe a flexible, computationally efficient approach for modeling large zero-inflated spatial data using the projection-based intrinsic conditional autoregression (PICAR) framework. We study our approach, which we call PICAR-Z, through extensive simulation studies and two environmental data sets. Our results suggest that PICAR-Z provides accurate predictions while remaining computationally efficient. An important goal of our work is to allow researchers who are not experts in computation to easily build computationally efficient extensions to zero-inflated spatial models; this also allows for a more thorough exploration of modeling choices in two-part models than was previously possible. We show that PICAR-Z is easy to implement and extend in popular probabilistic programming languages such as `nimble` and `stan`.

arXiv:2304.02476v1 [stat.ME] 5 Apr 2023

*Corresponding Author: Department of Statistics, George Mason University; 4400 University Drive, MS 4A7; Fairfax, VA 22030-4444; United States of America (e-mail: slee287@gmu.edu)

1 Introduction

Zero-inflated spatial data are spatially dependent observations characterized by an excess of zeros. Zero-inflated spatial data are common in many disciplines; for example, counts of harbor seals on glacial ice (Ver Hoef and Jansen, 2007), annual mental health expenditures among US federal employees (Neelon et al., 2011), and the number of torrential rainfall events in a region of interest (Lee and Kim, 2017). These data are typically a mixture of zeros and either discrete counts or positive real numbers. Standard probability distributions may not be appropriate for modeling zero-inflated data as they are unable to account effectively for the excess zeros (cf. Agarwal et al., 2002; Rathbun and Fei, 2006; Lambert, 1992).

A class of parametric mixture distributions called *two-part models* (Mullahy, 1986; Lambert, 1992) are popular for modeling zero-inflated data. Two-part models account for both the excess zeros and the skewed distribution of non-zero values by using two latent random variables, one for occurrence and the other for prevalence. The occurrence process dictates whether a structural zero or non-zero value is observed, and the prevalence process determines the value of the structural non-zero observations. Two-part models have been extended to model zero-inflated spatial observations (cf. Agarwal et al., 2002; Ver Hoef and Jansen, 2007; Olsen and Schafer, 2001) where the occurrence and prevalence random variables vary with respect to space (i.e. they are spatial random processes). Spatial two-part models are an extension of the well-known spatial generalized linear mixed models (SGLMMs) (Diggle et al., 1998), albeit with two separate latent spatial processes.

Modeling large zero-inflated spatial datasets remains a key challenge from both a computational and modeling standpoint. First, fitting spatial two-part models can be computationally prohibitive for large datasets because these models are generally overparameterized (Recta et al., 2012; Ver Hoef and Jansen, 2007) with more unknown parameters than observations. For high-dimensional data, model-fitting can be computationally

burdensome due to large matrix operations, estimation of high-dimensional latent random effects, and slow mixing Markov Chain Monte Carlo (MCMC) algorithms. Second, the underlying occurrence and prevalence spatial processes may potentially exhibit complex spatial dependence characteristics such as non-stationarity and anisotropy. Third, the occurrence and prevalence processes may be strongly correlated, and directly modeling the cross-correlations can be computationally expensive (Recta et al., 2012).

Novel modeling approaches for zero-inflated spatial data have been proposed, but these methods may not scale to larger datasets. In non-spatial settings, Frequentist methods have been used to fit two-part models using Gauss-Hermite quadrature (Min and Agresti, 2005), expectation-maximization (Lambert, 1992; Roeder et al., 1999), and restricted maximum quasi-likelihoods (Kim et al., 2012). However, these methods do not address a key component of spatial two-part models - inference for the two n -dimensional vectors of latent spatial random effects from the occurrence and prevalence spatial processes. Lyashevskaya et al. (2016) employs a Monte Carlo maximum likelihood approach to model a moderately large zero-inflated spatial dataset ($n = 4,029$), but this approach still requires estimation of the high-dimensional spatial random effects and costly matrix operations.

In the Bayesian framework, the literature primarily focuses on the sophistication of zero-inflated spatial models. However, there is a dearth of studies examining the computational issues associated with large zero-inflated spatial datasets. Studies have modeled spatio-temporal dependence (Fernandes et al., 2009; Neelon et al., 2016a; Arcuti et al., 2016), addressed overdispersion (Gschlößl and Czado, 2008; Lee et al., 2016), used skewed distributions (Dreassi et al., 2014; Liu et al., 2016), used t-distributions to model heavy tailed behavior (Neelon et al., 2015), and modeled prevalence with scale mixtures of normal distributions (Fruhworth-Schnatter and Pyne, 2010) or Student-t processes (Bopp et al., 2020). Another study facilitates posterior sampling for zero-inflated negative binomial distributions (ZINB) by using latent variables that are represented as scale mixtures of normal distributions (Neelon, 2019). A notable exception is Wang et al. (2015), which models the presence and abundance of Atlantic cod in 1325 locations along

the Gulf of Maine using predictive processes (Banerjee et al., 2008). Predictive processes still requires $\mathcal{O}(nm^2 + m^3)$ operations where m is the number of knots and n is the dataset size, and careful attention must be paid to knot selection (Guhaniyogi et al., 2011).

In this study, we introduce a computationally efficient approach for fitting a broad range of two-part models to high-dimensional zero-inflated spatial data. We use projection-based intrinsic conditional autoregression (PICAR) (Lee and Haran, 2021) to reduce the dimensions of and correlation between the spatial random effects in two-part spatial models. The PICAR method represents the spatial random effects using empirical basis functions based on the Moran’s I statistic and piecewise linear basis functions. Various basis representations have been directly or indirectly used to model spatial data; for instance, predictive processes (Banerjee et al., 2008), random projections (Guan and Haran, 2018, 2019; Banerjee et al., 2013; Park and Haran, 2020), Moran’s basis for areal models (Hughes and Haran, 2013), stochastic partial differential equations (Lindgren et al., 2011), kernel convolutions (Higdon, 1998), eigenvector spatial filtering (Griffith, 2003), and multi-resolution basis functions (Nychka et al., 2015; Katzfuss, 2017), among others. To our knowledge, this is the first approach that readily lends itself to wide range of user-specified spatial two-part models while also reducing computational costs for large datasets. We demonstrate the applicability of our proposed approach (PICAR-Z) via simulation studies as well as two real-world applications - a bivalve species abundance dataset and ice thickness measurements in West Antarctica. Because our approach allows for efficient inference, it allows us to more thoroughly explore the advantages (and disadvantages) various modeling choices in two-part models than was previously possible.

The rest of the manuscript is as follows. In Section 2, we introduce the general two-part modeling framework for zero-inflated data. We also provide an overview of spatial two-part models and examine the inherent modeling and computational challenges. In section 3, we propose a computationally efficient approach to fit high-dimensional spatial two-part models (PICAR-Z) and provide some implementation guidelines. We demonstrate the utility of PICAR-Z through four different simulation studies in Section

4 as well as two high-dimensional environmental datasets in Section 5. Finally, a summary and directions for future research are provided in Section 6.

2 Zero-inflated Spatial Models

In this section, we provide an overview of the two-part modeling framework (Mullahy, 1986; Lambert, 1992) for spatially dependent zero-inflated observations (cf. Ver Hoef and Jansen, 2007; Neelon et al., 2016a; Wang et al., 2015). Let $Z(\mathbf{s})$ be a zero-inflated observation for spatial location $\mathbf{s} \subset \mathcal{D}$ within the spatial domain $\mathcal{D} \in \mathbb{R}^2$. In the spatial two-part modeling framework, $Z(\mathbf{s})$ are generated as follows.

$$Z(\mathbf{s}) = \begin{cases} 0 & \text{if } O(\mathbf{s}) = 0 \\ P(\mathbf{s}) & \text{if } O(\mathbf{s}) = 1. \end{cases}, \quad (1)$$

where $O(\mathbf{s})$ and $P(\mathbf{s})$ are the spatial occurrence and prevalence processes respectively. The occurrence process is typically specified as $O(\mathbf{s}) \sim \text{Bern}(\cdot|\pi(\mathbf{s}))$ with spatially varying probabilities $\pi(\mathbf{s}) \in (0, 1)$. The prevalence process is modeled as $P(\mathbf{s}) \sim \tilde{F}(\cdot|\boldsymbol{\theta}(\mathbf{s}))$ where $\tilde{F}(\cdot|\boldsymbol{\theta}(\mathbf{s}))$ is a discrete or continuous probability distribution with spatially-varying parameters $\boldsymbol{\theta}(\mathbf{s})$. The key distinction from the univariate case is that the occurrence O and prevalence P random variables now vary across space; hence, we model the occurrence and prevalence as spatial random processes $O(\mathbf{s})$ and $P(\mathbf{s})$.

Spatial two-part models typically fall into two classes - hurdle and mixture models. In *hurdle models*, the occurrence random process $O(\mathbf{s})$ specifies which locations are associated with zero- or non-zero values. For the non-zero data, their respective positive values are generated by the prevalence random process $P(\mathbf{s})$. In the discrete case, $\tilde{F}(\cdot|\boldsymbol{\theta}(\mathbf{s}))$ is a zero-truncated probability mass function such as the zero-truncated Poisson or the zero-truncated negative binomial distribution. For semi-continuous observations, $\tilde{F}(\cdot|\boldsymbol{\theta}(\mathbf{s}))$ can be a probability density function with positive support such as a log-normal or gamma distribution. For *mixture models*, the zero-valued observations can be generated by both

processes $O(\mathbf{s})$ and $P(\mathbf{s})$. Here, $O(\mathbf{s})$ determines whether a location is classified as a structural zero or non-zero case. For the structural non-zero cases, the prevalence random process $P(\mathbf{s})$ generates both zeros and positive values. In the discrete case, $\tilde{F}(\cdot|\boldsymbol{\theta}(\mathbf{s}))$ is a non-degenerate mass function such as the Poisson or Negative-Binomial distribution. For semi-continuous observations, $\tilde{F}(\cdot|\boldsymbol{\theta}(\mathbf{s}))$ can be a censored model such as a Tobit Type I.

2.1 Modeling Framework: Spatial Two-Part Models

Here, we outline the general hierarchical modeling framework for spatial two-part models. The occurrence process $O(\mathbf{s})$ corresponds to the Bernoulli probability distribution with either a probit or a logit link function. The prevalence process $P(\mathbf{s})$ employs the appropriate probability distribution based on the observation class (discrete vs. semi-continuous) and zero-inflation structure (hurdle vs. mixture). For hurdle models, a zero-truncated distribution (e.g., zero-truncated Poisson, zero-truncated negative binomial, lognormal, or gamma) is a sensible choice for $\tilde{F}(\cdot|\boldsymbol{\theta})$. Mixture models utilize a distribution with non-negative support (e.g., Poisson, negative binomial, or Tobit Type I). For both processes, their respective linear predictors ($\boldsymbol{\eta}_o$ and $\boldsymbol{\eta}_p$) include the fixed and spatial random effects. The linear predictor for the occurrence process is $\boldsymbol{\eta}_o = \mathbf{X}\boldsymbol{\beta}_o + \mathbf{W}_o + \boldsymbol{\epsilon}_o$, where $\boldsymbol{\beta}_o$ and \mathbf{W}_o are the vectors of the fixed effects and spatial random effects, respectively, and $\boldsymbol{\epsilon}_o$ are the iid observational errors. The linear predictor for the prevalence process $\boldsymbol{\eta}_p$ can be constructed similarly to $\boldsymbol{\eta}_o$. The latent spatial random sub-processes $W_o(\mathbf{s})$ and $W_p(\mathbf{s})$ can be modeled as a stationary zero-mean Gaussian process with a Matérn covariance function (Stein, 2012), a widely used class of stationary and isotropic covariance functions. Link functions $g_o(\cdot)$ and $g_p(\cdot)$ are specified according to the spatial processes. To complete the Bayesian hierarchical model, we designate prior distributions for the model parameters.

The Bayesian hierarchical framework for spatial two-part models is:

$$\begin{aligned}
\text{Data Model:} \quad & \mathbf{Z}|O(\mathbf{s}), P(\mathbf{s}) \sim F(\cdot | O(\mathbf{s}), P(\mathbf{s})) & (2) \\
\text{Process Model:} \quad & O(\mathbf{s})|\pi(\mathbf{s}) \sim \text{Bern}(\cdot|\pi(\mathbf{s})) \\
& P(\mathbf{s})|\theta(\mathbf{s}) \sim \tilde{F}(\cdot|\theta(\mathbf{s})) \\
\text{Sub-process Model 1:} \quad & \pi(\mathbf{s})|\eta_o(\mathbf{s}) = g_o^{-1}(\eta_o(\mathbf{s})) \\
\text{(Occurrence)} \quad & \eta_o(\mathbf{s})|\boldsymbol{\beta}_o, W_o(\mathbf{s}), \epsilon_o(s) = \mathbf{X}(\mathbf{s})'\boldsymbol{\beta}_o + W_o(\mathbf{s}) + \epsilon_o(\mathbf{s}) \\
& \mathbf{W}_o = (W_o(\mathbf{s}_1), \dots, W_o(\mathbf{s}_n))' \\
& \mathbf{W}_o|\phi_o, \sigma_o^2 \sim \mathcal{N}(\mathbf{0}, \sigma_o^2 \mathbf{R}_{\phi_o}), \\
& \epsilon(s)|\tau_o^2 \sim \mathcal{N}(0, \tau_o^2) \\
\text{Sub-process Model 2:} \quad & \theta(\mathbf{s})|\eta_p(\mathbf{s}) = g_p^{-1}(\eta_p(\mathbf{s})) \\
\text{(Prevalence)} \quad & \eta_p(\mathbf{s})|\boldsymbol{\beta}_p, W_p(\mathbf{s}), \epsilon_p(\mathbf{s}) = \mathbf{X}(\mathbf{s})\boldsymbol{\beta}_p + W_p(\mathbf{s}) + \epsilon_p(\mathbf{s}) \\
& \mathbf{W}_p = (W_p(\mathbf{s}_1), \dots, W_p(\mathbf{s}_n))' \\
& \mathbf{W}_p|\phi_p, \sigma_p^2 \sim \mathcal{N}(\mathbf{0}, \sigma_p^2 \mathbf{R}_{\phi_p}) \\
& \epsilon(\mathbf{s})|\tau_p^2 \sim \mathcal{N}(0, \tau_p^2) \\
\text{Parameter Model:} \quad & \boldsymbol{\beta}_o \sim p(\boldsymbol{\beta}_o), \quad \boldsymbol{\beta}_p \sim p(\boldsymbol{\beta}_p), \quad \phi_o \sim p(\phi_o), \quad \phi_p \sim p(\phi_p) \\
& \sigma_o^2 \sim p(\sigma_o^2), \quad \sigma_p^2 \sim p(\sigma_p^2), \quad \tau_o^2 \sim p(\tau_o^2), \quad \tau_p^2 \sim p(\tau_p^2)
\end{aligned}$$

where $F(\cdot | O(\mathbf{s}), P(\mathbf{s}))$ is the distribution function of a spatial two-part model. From Equation 2, the likelihood function $f(z|O(\mathbf{s}), P(\mathbf{s}))$ is defined as:

$$f(z|O(\mathbf{s}), P(\mathbf{s})) = \begin{cases} \pi(\mathbf{s}) + (1 - \pi(\mathbf{s})) \times \tilde{f}(0; \theta(\mathbf{s})), & \text{if } z = 0 \\ (1 - \pi(\mathbf{s})) \times \tilde{f}(z; \theta(\mathbf{s})), & \text{if } z > 0. \end{cases}, \quad (3)$$

where $\pi(\mathbf{s})$ and $\theta(\mathbf{s})$ are the spatially-varying occurrence probabilities and prevalence intensities, respectively, and $\tilde{f}(z; \theta(\mathbf{s}))$ is the density function of the prevalence process.

The spatial two-part models fall into two classes (hurdle and mixture models). The

key difference between both classes lies in the choice of $\tilde{F}(\cdot|\theta(\mathbf{s}))$, the distribution of the prevalence process $P(\mathbf{s})$. Here, we introduce four commonly-used spatial two-part models and provide a summary in Table 7.

Hurdle Model for Spatial Count Data

The hurdle count model is a sensible two-part model for spatial zero-inflated data. This model assumes the occurrence process $O(\mathbf{s})$ solely generates zero-valued data; hence, the distribution of the prevalence process $\tilde{F}(\cdot|\theta(\mathbf{s}))$ is typically zero-truncated distribution such as a zero-truncated Poisson distribution, zero-truncated Negative binomial, or a translated Poisson distribution (Ver Hoef and Jansen, 2007). For the zero-truncated Poisson distribution, the likelihood function of the hurdle count model is defined as:

$$f(z|O(\mathbf{s}), P(\mathbf{s})) = \begin{cases} \pi(\mathbf{s}), & \text{if } z = 0 \\ (1 - \pi(\mathbf{s})) \times \frac{\theta(\mathbf{s})^z e^{-\theta(\mathbf{s})}}{z!(1 - e^{-\theta(\mathbf{s})})}, & \text{if } z > 0. \end{cases} \quad (4)$$

where $\pi(\mathbf{s}) = g_o^{-1}(\mathbf{X}(\mathbf{s})'\boldsymbol{\beta}_o + W_o(\mathbf{s}) + \epsilon_o(\mathbf{s}))$ is the occurrence probability process, and $\theta(\mathbf{s}) = \exp\{\mathbf{X}(\mathbf{s})'\boldsymbol{\beta}_p + \mathbf{W}_p(\mathbf{s}) + \epsilon_p(\mathbf{s})\}$ is the intensity process.

Hurdle Model for Spatial Semi-continuous Data

For semi-continuous observations, an appropriate two-part model is a hurdle model based on a continuous distribution over strictly positive real numbers. Similar to the discrete case, the hurdle model assumes the zero-valued data are generated from occurrence process $O(\mathbf{s})$ only. Common choices for the distribution of $P(\mathbf{s})$ are the lognormal, skewed-normal, truncated normal, and log-skew-t (Neelon et al., 2016b; Chai and Bailey, 2008). A popular example is the Bernoulli-lognormal hurdle model with likelihood function:

$$f(z|O(\mathbf{s}), P(\mathbf{s})) = \begin{cases} \pi(\mathbf{s}), & \text{if } z = 0 \\ (1 - \pi(\mathbf{s})) \times LN(z|\theta(\mathbf{s})), & \text{if } z > 0, \end{cases} \quad (5)$$

where $LN(z|\theta(\mathbf{s})) = \frac{1}{z\sqrt{2\pi\tau^2}} \exp\left(-\frac{(\ln z - \mu(\mathbf{s}))^2}{2\tau^2}\right)$ is the probability density function of a lognormal distribution with parameters $\theta(\mathbf{s}) = \{\mu(\mathbf{s}), \tau^2\}$. $\pi(\mathbf{s})$ can be modeled similarly as in the hurdle count model. However, the spatially-varying mean process is modeled as $\mu(\mathbf{s}) = \exp(\mathbf{X}(\mathbf{s})'\boldsymbol{\beta}_p + \mathbf{W}_p(\mathbf{s}) + \epsilon_p(\mathbf{s}))$.

Mixture Model for Spatial Count Data

The spatial zero-inflated mixture model is appropriate for modeling zero-inflated count data where both the occurrence $O(\mathbf{s})$ and prevalence processes $P(\mathbf{s})$ generate zero-values. $\tilde{F}(\cdot|\theta(\mathbf{s}))$ is typically a discrete distribution whose support is the non-negative integers (e.g. Poisson or Negative-Binomial distribution). A commonly-used case is the zero-inflated Poisson (ZIP) model, which utilizes the Poisson distribution. The corresponding likelihood function is:

$$f(z|O(\mathbf{s}), P(\mathbf{s})) = \begin{cases} \pi(\mathbf{s}) + (1 - \pi(\mathbf{s}))e^{-\theta(\mathbf{s})}, & \text{if } z = 0 \\ (1 - \pi(\mathbf{s}))\frac{\theta(\mathbf{s})^z e^{-\theta(\mathbf{s})}}{z!}, & \text{if } z > 0. \end{cases} \quad (6)$$

where $\pi(\mathbf{s})$ is modeled similarly as in the previous cases, and the spatially-varying intensity process $\theta(\mathbf{s})$ is modeled as $\theta(\mathbf{s}) = \exp\{\mathbf{X}(\mathbf{s})'\boldsymbol{\beta}_p + \mathbf{W}_p(\mathbf{s}) + \epsilon_p(\mathbf{s})\}$.

Mixture Model for Spatial Semi-continuous Data

Mixture models can also be extended to spatial zero-inflated semi-continuous data where both the occurrence $O(\mathbf{s})$ and prevalence processes $P(\mathbf{s})$ generate zeros. For this class of models, the prevalence process $P(\mathbf{s})$ generally includes a censored distribution such as a Type 1 Tobit model (Tobin, 1958; Moulton and Halsey, 1995) to generate ‘censored’ zeros and positive values. One example is the zero-inflated Tobit (ZIT) two-part model. The Type 1 Tobit model generates censored data $P(\mathbf{s}) \in \{0, \mathbb{R}^+\}$ as follows:

$$P(\mathbf{s}) = \begin{cases} P^*(\mathbf{s}), & \text{if } P^*(\mathbf{s}) > \gamma \\ 0, & \text{if } P^*(\mathbf{s}) \leq \gamma \end{cases}, \quad (7)$$

where γ is a threshold (or lower detection limit) and $P^*(\mathbf{s})$ is an auxiliary latent random variable where $P^*(\mathbf{s}) \sim \mathcal{N}(\mu(\mathbf{s}), \tau^2)$. For a threshold γ , we have the following likelihood function $f_Z(z; \theta(s))$:

$$f_Z(z; \theta) = \begin{cases} \Phi\left(\frac{\gamma - \mu(s)}{\tau}\right), & \text{if } z = 0 \\ \frac{1}{\tau} \phi\left(\frac{z - \mu(s)}{\tau}\right), & \text{if } z > 0. \end{cases}, \quad (8)$$

where $\Phi(\cdot)$ is the standard normal cumulative distribution function and $\phi(\cdot)$ is the standard normal probability density function. The estimable model parameters are $\theta(s) = \{\mu(s), \tau^2\}$, and the likelihood function for the zero-inflated Tobit (ZIT) model is:

$$f(z|O(\mathbf{s}), P(\mathbf{s})) = \begin{cases} \pi(\mathbf{s}) + (1 - \pi(\mathbf{s})) \times \Phi\left(\frac{\gamma - \mu(\mathbf{s})}{\tau}\right), & \text{if } z = 0 \\ (1 - \pi(\mathbf{s})) \times \frac{1}{\tau} \phi\left(\frac{z - \mu(\mathbf{s})}{\tau}\right), & \text{if } z > 0. \end{cases}, \quad (9)$$

where $\Phi(\cdot)$ and $\phi(\cdot)$ are the cumulative distribution function and the probability density function of a standard normal distribution. We model the spatially-varying occurrence process $\pi(\mathbf{s})$ in the same way as in the previous cases, and the mean process is modeled as $\mu(\mathbf{s}) = \mathbf{X}(\mathbf{s})'\boldsymbol{\beta}_P + \mathbf{W}_p(\mathbf{s}) + \epsilon_p(\mathbf{s})$.

2.2 Computational Challenges

Spatial two-part models are subject to computational obstacles in the high-dimensional setting. Both the occurrence $O(\mathbf{s})$ and prevalence $P(\mathbf{s})$ processes include latent spatial random fields, which can be computationally prohibitive to model for even moderately large datasets (more than 1000 observations) (Haran, 2011). These require a costly evaluation of an n -dimensional multivariate normal likelihood function with $\mathcal{O}(n^3)$ operations at each iteration of the MCMC algorithm. The highly correlated spatial random effects can result in poor mixing Markov chains (cf. Christensen et al., 2006; Haran et al., 2003). Another consideration is modeling the cross-covariance between the occurrence and prevalence processes, which also requires expensive matrix inversions and computing determinants (Recta et al., 2012).

Past studies employed Guass-Hermite quadrature (Min and Agresti, 2005), expectation-

maximization (Lambert, 1992; Roeder et al., 1999), or restricted maximum quasi-likelihoods (Kim et al., 2012) to fit zero-inflated models. However, such approximations may not scale well with high-dimensional random effects (Neelon et al., 2016b) that exhibit spatial correlation. In the spatial setting, Monte Carlo Maximum Likelihood (Lyashevskaya et al., 2016) and predictive processes (Wang et al., 2015) have been incorporated into the two-part modeling framework. Yet, these approaches are still computationally costly and they may not scale well to larger datasets. For instance, Lyashevskaya et al. (2016) required over 72 hours to model 4029 zero-inflated spatial observations. Wang et al. (2015) models a dataset with 1325 locations using predictive processes (Banerjee et al., 2008), which scales at $\mathcal{O}(nm^2 + m^3)$ where n is the number of observed locations and m denotes the number of knot locations. Selecting the proper knot locations (Guhaniyogi et al., 2011) can be challenging.

3 A Computationally Efficient Approach for Fitting Two-Part Models

In this section, we propose a scalable method (PICAR-Z) for fitting high-dimensional spatial two-part models. Our approach builds upon the projection-based intrinsic conditional autoregression (PICAR) framework (Lee and Haran, 2021). PICAR-Z approximates the latent spatial occurrence $O(\mathbf{s})$ and prevalence $P(\mathbf{s})$ processes through a basis expansion of the Moran’s basis functions. We present the general hierarchical modeling framework, practical guidelines for implementation, and a discussion of the computational speedup associated with PICAR-Z.

Consider the vector of spatial random effects $\mathbf{W} = (W(\mathbf{s}_1), \dots, W(\mathbf{s}_n))'$, which can be approximated as a linear combination of spatial basis functions: $\mathbf{W} \approx \mathbf{\Phi}\boldsymbol{\delta}$ where $\mathbf{\Phi}$ is an $n \times p$ basis function matrix where each column denotes a basis function, $\boldsymbol{\delta} \in \mathbb{R}^p$ are the re-parameterized spatial random effects (or basis coefficients). Moreover, $\boldsymbol{\delta} \sim \mathcal{N}(0, \Sigma_\delta)$ where Σ_δ is the $p \times p$ covariance matrix for the coefficients. Basis functions can be

interpreted as a set of distinct spatial patterns and a weighted sum of these patterns can construct a spatial random field. Basis representation has been a popular approach to model spatial data (cf. Cressie and Johannesson, 2008; Banerjee et al., 2008; Hughes and Haran, 2013; Lindgren et al., 2011; Rue et al., 2009; Haran et al., 2003; Griffith, 2003; Higdon, 1998; Nychka et al., 2015). Basis representations tend to be computationally efficient (Cressie and Wikle, 2015) as they help bypass large matrix operations and reduce the dimensions of and correlation among the spatial random effects.

3.1 Projection Intrinsic Autoregression (PICAR)

The projection-based intrinsic conditional auto-regression (PICAR) approach consists of three components: (1) generate a triangular mesh on the spatial domain $\mathcal{D} \subset \mathbb{R}^2$; (2) construct a spatial field on the mesh vertices using non-parametric basis functions; (3) interpolate onto the observation locations using piece-wise linear basis functions.

Mesh Construction

Prior to fitting the model, we generate a mesh enveloping the observed spatial locations via Delaunay Triangulation (Hjelle and Dæhlen, 2006). Next, the the spatial domain D is partitioned into a collection of non-intersecting irregular triangles. The triangles can share a common edge, corner (i.e. nodes or vertices), or both. The mesh generates a latent undirected graph $G = \{V, E\}$, where $V = \{1, 2, \dots, m\}$ are the mesh vertices and E are the edges. Each edge E is represented as a pair (i, j) denoting the connection between i and j . The graph G is characterized by its weights matrix \mathbf{N} , an $m \times m$ matrix where $N_{ii} = 0$ and $N_{ij} = 1$ when mesh node i is connected to node j and $N_{ij} = 0$ otherwise. The triangular mesh can built using the **R-INLA** package (Lindgren et al., 2015).

Moran’s Basis Functions

Next, we construct the Moran’s basis functions (Hughes and Haran, 2013; Griffith, 2003) on the set of mesh vertices V of graph G . The Moran’s basis functions refer to the leading

p eigenvectors of the Moran's operator $(\mathbf{I} - \mathbf{1}\mathbf{1}'/m)\mathbf{N}(\mathbf{I} - \mathbf{1}\mathbf{1}'/m)$, where \mathbf{I} is the identity matrix and $\mathbf{1}$ is a vector of 1's. Note that this operator is a component of the Moran's I statistic:

$$I(A) = \frac{m}{\mathbf{1}'\mathbf{N}\mathbf{1}} \frac{\mathbf{Z}'(\mathbf{I} - \mathbf{1}\mathbf{1}'/m)\mathbf{N}(\mathbf{I} - \mathbf{1}\mathbf{1}'/m)\mathbf{Z}}{\mathbf{Z}'(\mathbf{I} - \mathbf{1}\mathbf{1}'/m)\mathbf{Z}},$$

a diagnostic of spatial dependence (Moran, 1950) used for areal spatial data. Values of the Moran's I above $-\frac{1}{m-1}$ indicate positive spatial autocorrelation and values below $-\frac{1}{m-1}$ indicate negative spatial autocorrelation (Griffith, 2003). For the triangular mesh, the positive eigenvectors represent the patterns of spatial clustering, or dependence, among the mesh nodes, and their corresponding eigenvalues denote the magnitude of clustering. We construct the Moran's basis function matrix $\mathbf{M} \in \mathbb{R}^{m \times p}$, by selecting the first p eigenvectors of the Moran's operator where $p \ll m$. Rank selection for p proceeds via an automated heuristic (Lee and Haran, 2021) based on out-of-sample validation. A spatial random field can be constructed through a linear combinations of the Moran's basis functions (contained in matrix \mathbf{M}) and their corresponding weights $\delta \in \mathbb{R}^p$.

Piece-wise Linear Basis Functions

To complete the PICAR approach, we introduce a set of piece-wise linear basis functions (Brenner and Scott, 2007) to interpolate points within the triangular mesh (i.e. the undirected graph $G = (V, E)$). Following Lee and Haran (2021), we construct a spatial random field on the mesh nodes $\tilde{\mathbf{W}} = (W(\mathbf{v}_1), \dots, W(\mathbf{v}_m))'$ where $\mathbf{v}_i \in V$ and then project, or interpolate, onto the observed locations $\mathbf{W} = (W(\mathbf{s}_1), \dots, W(\mathbf{s}_n))'$ where $\mathbf{s}_i \in \mathcal{D}$. The latent spatial random field \mathbf{W} can be represented as $\mathbf{W} = \mathbf{A}\tilde{\mathbf{W}}$, where \mathbf{A} is an $n \times m$ projector matrix containing the piece-wise linear basis functions. The rows of \mathbf{A} correspond to an observation location $\mathbf{s}_i \in \mathcal{D}$, and the columns correspond to a mesh node $\mathbf{v}_i \in V$. The i th row of \mathbf{A} contains the weights to linearly interpolate $W(\mathbf{s}_i)$. In practice, we use an $n \times m$ projector matrix \mathbf{A} for fitting the hierarchical spatial model. For model validation and prediction, we generate an $n_{CV} \times m$ projector matrix \mathbf{A}_{CV} that interpolates onto the n_{CV} validation locations.

3.2 PICAR Approach for Zero-inflated Spatial Data

The PICAR approach readily extends to spatial two-part models (Equation 2). Using PICAR, we approximate both the latent spatial occurrence $O(\mathbf{s})$ and prevalence $P(\mathbf{s})$ processes as an expansion of Moran's basis functions (Griffith, 2003; Hughes and Haran, 2013). PICAR-Z approximates the spatial random effects for the occurrence and prevalences processes, respectively, as $\mathbf{W}_o \approx \mathbf{A}_o \mathbf{M}_o \boldsymbol{\delta}_o$ and $\mathbf{W}_p \approx \mathbf{A}_p \mathbf{M}_p \boldsymbol{\delta}_p$ using projector matrices \mathbf{A}_o and \mathbf{A}_p , Moran's basis functions matrices \mathbf{M}_o and \mathbf{M}_p , and basis coefficients $\boldsymbol{\delta}_o$ and $\boldsymbol{\delta}_p$. The PICAR-Z hierarchical framework for spatial two-part models is:

$$\begin{aligned}
 \text{Data Model:} & \quad Z(\mathbf{s})|O(\mathbf{s}), P(\mathbf{s}) \sim F(\cdot | O(\mathbf{s}), P(\mathbf{s})) \\
 \text{Process Model:} & \quad O(\mathbf{s})|\pi(\mathbf{s}) \sim \text{Bern}(\pi(\mathbf{s})) \\
 & \quad P(\mathbf{s})|\theta(\mathbf{s}) \sim \tilde{F}(\cdot|\theta(\mathbf{s})) \\
 \text{Sub-process Model 1:} & \quad \pi(\mathbf{s})|\eta_o(\mathbf{s}) = g_o^{-1}(\eta_o(\mathbf{s})) \\
 \text{(Occurrence)} & \quad \eta_o(\mathbf{s})|\boldsymbol{\beta}_o, \boldsymbol{\delta}_o = \mathbf{X}(\mathbf{s})'\boldsymbol{\beta}_o + [\mathbf{A}_o \mathbf{M}_o \boldsymbol{\delta}_o](\mathbf{s}) \\
 & \quad \boldsymbol{\delta}_o|\tau_o \sim \mathcal{N}(\mathbf{0}, \tau_o^{-1}(\mathbf{M}_o' \mathbf{Q}_o \mathbf{M}_o)^{-1}) \\
 \text{Sub-process Model 2:} & \quad \theta(\mathbf{s})|\eta_p(\mathbf{s}) = g_p^{-1}(\eta_p(\mathbf{s})) \\
 \text{(Prevalence)} & \quad \eta_p(\mathbf{s})|\boldsymbol{\beta}_p, \boldsymbol{\delta}_p = \mathbf{X}(\mathbf{s})'\boldsymbol{\beta}_p + [\mathbf{A}_p \mathbf{M}_p \boldsymbol{\delta}_p](\mathbf{s}) \\
 & \quad \boldsymbol{\delta}_p|\tau_p \sim \mathcal{N}(\mathbf{0}, \tau_p^{-1}(\mathbf{M}_p' \mathbf{Q}_p \mathbf{M}_p)^{-1}), \\
 \text{Parameter Model:} & \quad \boldsymbol{\beta}_o \sim \mathcal{N}(\boldsymbol{\mu}_{\beta_o}, \Sigma_{\beta_o}), \quad \boldsymbol{\beta}_p \sim \mathcal{N}(\boldsymbol{\mu}_{\beta_p}, \Sigma_{\beta_p}) \\
 & \quad \tau_o \sim \mathcal{G}(\alpha_{\tau_o}, \beta_{\tau_o}), \quad \tau_p \sim \mathcal{G}(\alpha_{\tau_p}, \beta_{\tau_p})
 \end{aligned}$$

where $F(\cdot | O(\mathbf{s}), P(\mathbf{s}))$ is the distribution of the specified two-part model such as the hurdle models (Equations 4 and 5) and mixture models (Equations 6 and 9). $\tilde{F}(\cdot|\theta(\mathbf{s}))$ denote the distribution function of the prevalence process. \mathbf{A}_o and \mathbf{A}_p are the projectors matrices for the occurrence and prevalence processes, respectively. For the occurrence and prevalence processes, we now incorporate the Moran's basis functions matrices \mathbf{M}_o and \mathbf{M}_p , the basis coefficients $\boldsymbol{\delta}_o$ and $\boldsymbol{\delta}_p$, and the precision parameters τ_o and τ_p . \mathbf{Q} , the

$m \times m$ prior precision matrix for the mesh vertices, is typically fixed prior to model fitting (see Lee and Haran (2021) for additional details). $[\mathbf{A}_o \mathbf{M}_o \boldsymbol{\delta}_o](\mathbf{s})$ denotes the value of the basis expansion $\mathbf{A}_o \mathbf{M}_o \boldsymbol{\delta}_o$ corresponding to location \mathbf{s} . The interpretation of $[\mathbf{A}_p \mathbf{M}_p \boldsymbol{\delta}_p]$ follows similarly.

The PICAR-Z approach is amenable to be modified to capture the cross-covariance between the occurrence $O(\mathbf{s})$ and prevalence $P(\mathbf{s})$ processes. Past studies have examined methodology for estimating the cross-covariance between two spatial random fields (Oliver, 2003; Recta et al., 2012). Recta et al. (2012) models the cross-correlation parameter ρ . We extend the general modeling framework from Recta et al. (2012) to high-dimensional settings by imposing correlation on the dimension-reduced Moran’s basis coefficients $\boldsymbol{\delta}_o$ and $\boldsymbol{\delta}_p$. We provide additional details for modeling the cross-correlation under the PICAR-Z framework in the supplement.

3.3 Tuning Mechanisms

Though most of the PICAR-Z approach is readily automated, there are key tuning mechanisms left to the practitioner: (1) selecting the rank of Moran’s basis functions matrices (p_o and p_p); (2) specifying the precision matrices of the mesh vertices (\mathbf{Q}_o and \mathbf{Q}_p); and (3) identifying the appropriate two-part model. Here, we examine these tuning mechanisms in detail and provide practical guidelines for implementation.

First, we provide an automated heuristic to select the appropriate ranks (p_o and p_p) of the Moran’s basis function matrices for both processes, \mathbf{M}_o and \mathbf{M}_p . First, we generate two augmented datasets, \mathbf{Z}_o^* and \mathbf{Z}_p^* , constructed from the original zero-inflated spatial dataset \mathbf{Z} . The first dataset is generated as:

$$Z_o^*(s) = \begin{cases} 0, & \text{if } Z(s) = 0 \\ 1, & \text{if } Z(s) > 0. \end{cases}, \quad (10)$$

The second dataset $\mathbf{Z}_p^* \in \mathbb{R}^{n_p}$ is the collection of all observations such that $Z(s) > 0$

and n_p corresponds to the sample size of \mathbf{Z}_p^* . Next, we generate a set \mathcal{P} consisting of h equally spaced points within the interval $[2, P]$ where P is the maximum rank and h is the interval resolution ($h = P - 1$ by default). Here, $P < m$ and both P and h are chosen by the user.

For the augmented dataset $\mathbf{Z}_o^*(\mathbf{s})$, we proceed in the following way. For each $p \in \mathcal{P}$, we construct an $n \times (k + p)$ matrix of augmented covariates $\tilde{\mathbf{X}}_o = [X \ \mathbf{A}_o \mathbf{M}_p]$ where $X \in \mathbb{R}^{n \times k}$ is the original covariate matrix, $\mathbf{A}_o \in \mathbb{R}^{n \times m}$ is the projector matrix, and $\mathbf{M}_p \in \mathbb{R}^{m \times p}$ are the leading p eigenvectors of the Moran's operator. Next, we use maximum likelihood approaches to fit the appropriate generalized linear model (GLM) for binary responses with a logit or probit link function. Finally, we set p_o to be the rank p that yields the lowest out-of-sample root mean squared prediction error (rmspe) or area under the ROC curve (AUC).

We implement a similar procedure for the second augmented dataset $\mathbf{Z}_p^* \in \mathbb{R}^{n_p}$. For each $p \in \mathcal{P}$, we construct an $n_p \times (k + p)$ matrix of augmented covariates $\tilde{\mathbf{X}}_p = \begin{bmatrix} \mathbf{X}_p & \mathbf{A}_p \mathbf{M}_p \end{bmatrix}$ where $\mathbf{X}_p \in \mathbb{R}^{n_p \times k}$ is the matrix of covariates, $\mathbf{A}_p \in \mathbb{R}^{n_p \times m}$ is the projector matrix, and $\mathbf{M}_p \in \mathbb{R}^{m \times p}$ are the leading p eigenvectors of the Moran's operator. Note that the rows of \mathbf{X}_p , \mathbf{A}_p , and \mathbf{M}_p correspond to the n_p locations with non-zero values. Next, we use maximum likelihood approaches to fit the appropriate generalized linear model (GLM) for positive responses. For count data, the likelihood function is a zero-truncated Poisson distribution. For semi-continuous data in the hurdle model framework, we employ a lognormal distribution as the likelihood function. For semi-continuous data in the mixture model framework, we simply fit the traditional linear model. Then, we set p_p to be the rank p that yields the lowest out-of-sample root mean squared prediction error (rmspe).

Next, we provide some choices for \mathbf{Q} , the prior precision matrix for the mesh vertices $\tilde{\mathbf{W}}$. By default, we set \mathbf{Q} to be the precision matrix of an intrinsic conditional auto-regressive model (ICAR). Similarly, we could set \mathbf{Q} as the precision matrix of a conditional auto-regressive model (CAR). Here, $\mathbf{Q} = (\mathbf{N}\mathbf{1} - \rho\mathbf{N})$, where N is the adjacency matrix

and $\rho \in (0, 1)$ is a predetermined correlation coefficient. It is possible to estimate ρ as a model parameter, but doing so requires an eigendecomposition of the Moran’s operator ($\mathcal{O}(m^3)$) at each iteration of the MCMC algorithm, which can negate the computational gains of the PICAR-Z approach. Another alternative is setting $\mathbf{Q} = I$, where the mesh nodes $\tilde{\mathbf{W}}$ and re-parameterized spatial random effects δ are uncorrelated.

Specifying the class (hurdle vs. mixture) of two-part model is an active area of research (cf. Feng, 2021; Vuong, 1989; Neelon et al., 2016b). Past studies have selected the appropriate model class using the Akaike Information Criterion (AIC) (Feng, 2021) or the Vuong test statistics (Vuong, 1989). However, the choice between a hurdle and mixture model depends on the aims of the investigator and prior scientific knowledge regarding the zero-generating processes (i.e. should the prevalence process also generate zeros). For practitioners, we suggest conducting a sensitivity analysis using both mixture and hurdle models, and then select the appropriate model based on out-of-sample validation. Since PICAR-Z is computationally efficient and scales to larger datasets, conducting such a sensitivity analysis should be feasible in many settings.

3.4 Computational Advantages

The PICAR-Z approach requires shorter walltimes per iteration (of the MCMC algorithm) as well as fewer iterations for the Markov chain to converge. The computational speedup results from exploiting lower-dimensional and weakly correlated basis coefficients δ_o and δ_p and also bypassing expensive matrix operations (e.g. Cholesky decompositions). The PICAR-Z approach has a computational complexity of $\mathcal{O}(2np)$ as opposed to $\mathcal{O}(2n^3)$ for the full hierarchical spatial two-part model.

We examine mixing in MCMC algorithms within the context of spatial two-part models. The PICAR-Z approach generates a faster mixing MCMC algorithm than fitting the full two-part model using the reparameterization method (gold standard) (Christensen and Waagepetersen, 2002) and a competing approach using bi-square basis functions (Cressie and Johannesson, 2008). This is corroborated by the larger effective sample size

per second (ES/sec), which approximates the rate at which samples are produced from an MCMC algorithm that are equivalent to samples from an IID sampler. Larger values of ES/sec indicates faster mixing. In the simulated examples (Section 4), the PICAR-Z approach returns a larger ES/sec than the gold standard across all model parameters and spatial random effects (see supplement).

For PICAR, the two major computational bottlenecks are constructing the Moran’s operator and computing its k -leading eigencomponents. The Moran’s operator requires the matrix operation $(\mathbf{I} - \mathbf{1}\mathbf{1}'/m)\mathbf{N}(\mathbf{I} - \mathbf{1}\mathbf{1}'/m)$ which results in $2m^3 - m^2$ floating point operations (FLOPs) where m is the number of mesh vertices. For dense mesh structures (large m), we can generate the Moran’s operator by leveraging the embarrassingly parallel operations as well the sparsity of the weights matrix \mathbf{N} . Next, the first k eigencomponents of the Moran’s Operator can be computed using a partial eigendecomposition approach such as the Implicitly Restarted Arnoldi Method (Lehoucq et al., 1998) from the **RSpectra** package (Qiu and Mei, 2019). Since the PICAR approach generally selects the leading p_o or p_p eigenvectors where $p_o \ll m$ and $p_p \ll m$, an expensive full eigendecomposition of the Moran’s operator is not necessary.

4 Simulation Study

In this section, we conduct an extensive simulation study focusing on four commonly-used spatial two-part models: (1) hurdle model with count data; (2) mixture model with count data; (3) hurdle model with semi-continuous data; and (4) mixture model with semi-continuous data. In addition, we provide comparisons to fixed rank kriging (Sengupta and Cressie, 2013; Cressie and Johannesson, 2008)) and a ‘gold standard’ method using reparameterization (Christensen and Waagepetersen, 2002).

4.1 Simulation Study Design

For all four two-part models, we simulate $B = 100$ samples for a total of $4 \times 100 = 400$ datasets in the simulation study. In each sample, we generate a set of 1400 randomly-selected locations on the unit domain $[0, 1]^2$. 1000 observations are allocated for model-fitting and the remaining 400 reserved for model validation. We chose a smaller sample size $n = 1000$ to allow for comparisons against a ‘gold standard’ method, which may be difficult to implement with larger datasets (see Section 2.2). Please see the supplement for details on the ‘gold standard’ approach.

For each sample, we randomly generate a matrix of covariates $\mathbf{X} = [\mathbf{X}_1, \mathbf{X}_2]$. We use the same regression coefficients $\boldsymbol{\beta}_o = \boldsymbol{\beta}_p = (1, 1)^T$ for all datasets in the simulation study. The spatial random effects \mathbf{W}_o and \mathbf{W}_p are generated from the multivariate Gaussian process proposed in Recta et al. (2012). Note that the prohibitively high computational costs made it challenging to explore model structures carefully and extend them to higher-dimensional settings.

$$\begin{bmatrix} \mathbf{W}_o \\ \mathbf{W}_p \end{bmatrix} \sim \mathcal{N} \left(\begin{bmatrix} \mathbf{0} \\ \mathbf{0} \end{bmatrix}, \begin{bmatrix} \mathbf{C}(\cdot|\nu_o, \phi_o, \sigma_o^2) & \rho \mathbf{L}_o \mathbf{L}_p^T \\ \rho \mathbf{L}_o \mathbf{L}_p^T & \mathbf{C}(\cdot|\nu_p, \phi_p, \sigma_p^2) \end{bmatrix} \right).$$

where $\mathbf{C}(\cdot|\nu_o, \phi_o, \sigma_o^2)$ and $\mathbf{C}(\cdot|\nu_p, \phi_p, \sigma_p^2)$ are covariance matrices for \mathbf{W}_o and \mathbf{W}_p , respectively. ρ represents cross-correlation between the occurrence and prevalence processes at the same location. We fix $\rho = 0.7$ to impose moderate positive cross-correlation between the occurrence and prevalence processes. \mathbf{L}_o and \mathbf{L}_p are the lower-triangular Choleski factors of $\mathbf{C}(\cdot|\nu_o, \phi_o, \sigma_o^2)$ and $\mathbf{C}(\cdot|\nu_p, \phi_p, \sigma_p^2)$, respectively. That is, $\mathbf{C}(\cdot|\nu_o, \phi_o, \sigma_o^2) = \mathbf{L}_o \mathbf{L}_o^T$ and $\mathbf{C}(\cdot|\nu_p, \phi_p, \sigma_p^2) = \mathbf{L}_p \mathbf{L}_p^T$. The covariance matrices, $\mathbf{C}(\cdot|\nu_o, \phi_o, \sigma_o^2)$ and $\mathbf{C}(\cdot|\nu_p, \phi_p, \sigma_p^2)$ are from the Matérn class (cf. Rasmussen and Williams, 2006; Rasmussen, 2004) of covariance functions with parameters $\nu_o = \nu_p = 0.5$, $\sigma_o^2 = \sigma_p^2 = 1$, and $\phi_o = \phi_p = 0.2$. We use the exponential covariance function ($\nu = 0.5$) to generate a ‘rough’ latent spatial process that is not mean square differentiable (Rasmussen, 2004).

We first generate realizations from the latent occurrence process $O(\mathbf{s})$ such that the underlying probability surface is modeled as $\pi(\mathbf{s}) = \text{logit}^{-1}(\mathbf{X}(\mathbf{s})'\boldsymbol{\beta}_O + \mathbf{W}_O)$. Next, we generate realizations from the prevalence process $P(\mathbf{s})$ from the corresponding prevalence distribution $\tilde{F}(\cdot|\theta(\mathbf{s}))$ (Equation 2) with spatially varying intensity (or mean) processes $\theta(\mathbf{s})$. We use a zero-truncated Poisson, Lognormal, Poisson, and Type I Tobit distribution for the hurdle count, hurdle semi-continuous, mixture count, and mixture semi-continuous cases, respectively. For the hurdle count and mixture count cases, we model the underlying intensity process as $\theta(\mathbf{s}) = \exp\{\mathbf{X}(\mathbf{s})'\boldsymbol{\beta}_P + \mathbf{W}_p(\mathbf{s})\}$. For the semi-continuous models, we specify $\theta(\mathbf{s}) = (\boldsymbol{\mu}(\mathbf{s}), \tau^2)$ with the mean process $\boldsymbol{\mu}(\mathbf{s}) = \mathbf{X}(\mathbf{s})'\boldsymbol{\beta}_P + \mathbf{W}_p(\mathbf{s})$ and nugget variance $\tau^2 = 0.1$. Finally, the observed data are drawn from the respective distribution of the spatial two-part model $F(\cdot|O(\mathbf{s}), P(\mathbf{s}))$.

Implementation and Competing Methods

To complete the hierarchical framework, we specify prior distributions for the zero-inflated spatial model parameters. We assign a multivariate normal prior for the regression coefficients where $\boldsymbol{\beta}_O \sim \mathcal{N}(\mathbf{0}, 100\mathbf{I})$ and $\boldsymbol{\beta}_P \sim \mathcal{N}(\mathbf{0}, 100\mathbf{I})$. For the variance of the spatial basis coefficients, we specify a non-informative inverse gamma priors where $\sigma_O^2 \sim \mathcal{IG}(0.002, 0.002)$ and $\sigma_P^2 \sim \mathcal{IG}(0.002, 0.002)$. The cross-correlation coefficient between the occurrence and prevalence processes ρ follows a uniform distribution $\rho \sim \mathcal{U}(-1, 1)$. For the semi-continuous cases, the nugget variance τ_ϵ^2 for the prevalence process follows an inverse gamma distribution $\tau_\epsilon^2 \sim \mathcal{IG}(0.002, 0.002)$. For the PICAR-Z approach, we ran 150,000 iterations of the MCMC algorithm. The MCMC algorithm is implemented using the programming language `nimble` (de Valpine et al., 2017).

We compare the PICAR-Z method against fixed rank kriging (Sengupta and Cressie, 2013; Cressie and Johannesson, 2008) as well as the ‘gold standard’ reparameterization approach (Christensen and Waagepetersen, 2002). Due to computational constraints, we elected to use the approach from Christensen and Waagepetersen (2002) over the full spatial hierarchical two-part model from Section 2.1. The reparameterization approach

is, by design, a computationally efficient method for modeling latent spatial random processes as it improves mixing in the MCMC algorithm by considerably reducing the correlation in the spatial random effects. For the ‘gold standard’ approach, we assume that the class of covariance function (Matérn) and the smoothness parameter ($\nu = 0.5$) are known a priori, which may not necessarily be the case in other scenarios. Additional details for the competing approaches are provided in the supplement.

We provide the following validation metrics averaged over all samples in the simulation study: (1) out-of-sample root mean squared prediction error (rmspe total) for all observations; (2) area under the receiver operating characteristic curve (AUC) for the zero-valued observations; and (3) rmspe for the non-zero-valued observations (rmspe positive). The AUC is used to assess how well each approach classifies zero-valued observations in a binary classification setting. The out-of-sample root mean squared prediction error (rmspe) is $\text{rmspe} = \sqrt{\frac{1}{n_{CV}} \sum_{i=1}^{n_{CV}} (Y_i^* - \hat{Y}_i^*)^2}$, where $n_{CV} = 400$, Y_i^* ’s denote the i -th value in the validation sample, and \hat{Y}_i^* ’s are the predicted values at the i -th location. In addition, we compare the computational walltimes to draw 150,000 samples from the respective posterior distributions via MCMC. We assess convergence of the Markov chains using the batch means standard errors. The computation times are based on a single 2.4 GHz Intel Xeon Gold 6240R processor. All the code was run on the George Mason University Office of Research Computing (ORC) HOPPER high-performance computing infrastructure.

4.2 Results

Table 7 contains the out-of-sample prediction results for the entire validation sample (rmspe), positive-valued observations (rmspe), and zero vs. non-zero values (AUC) as well as the average model-fitting walltimes. Results of the simulation study suggest that PICAR-Z outperforms both the competing approach (fixed rank kriging) and the ‘gold standard’ in prediction across all four classes of two-part models (see Table 7). All approaches perform comparably for binary classification of the zero vs. non-zero

cases, as corroborated by similar AUC values. However, the PICAR-Z methods (with and without cross-correlation) provide more accurate predictions for the non-zero (i.e. positive-valued) observations, in comparison to the other two methods. Estimating the correlation parameter does not strongly affect accuracy, save for the semi-continuous hurdle case. Note that the PICAR-Z approach outperformed the ‘gold standard’ method in predictive performance, which is consistent with results from past studies that examined basis representations of spatial latent fields (Bradley et al., 2019; Lee and Haran, 2021). Figure 7 provides a visual representation of the latent probability $\pi(\mathbf{s})$ and log-intensity $\log(\theta(\mathbf{s}))$ surfaces.

We also consider mixing in MCMC algorithms by examining the effective sample size per second (ES/sec), or the rate at which independent samples are generated by the MCMC algorithm. Larger values of ES/sec are indicative of faster mixing Markov chains. Note that PICAR-Z approach generates a faster mixing MCMC algorithm than the reparameterization method (Rep-SGLMM) (Christensen and Waagepetersen, 2002), an method specifically designed to improve mixing for SGLMMs. For model parameters β_{1o} , β_{2o} , β_{1p} , and β_{1p} , PICAR-Z yields an ES/sec of 218.89, 214.15, 44.00, and 43.83, respectively. The gold standard returns an ES/sec 0.66, 0.63, 0.26, and 0.25, respectively. For the spatial random effects $\mathbf{W}_o(s)$ and $\mathbf{W}_p(s)$, the median ES/sec is 53.09 and 28.70 for the PICAR-Z approach and 0.71 and 0.40 for the gold standard, an improvement by a factor of roughly 74.3 and 72.5. Across all four model classes, the PICAR-Z approach has shorter walltimes to run 150,000 iterations of the Metropolis-Hastings algorithm than fixed-rank kriging (bisquare) and the ‘gold’ standard (Table 7). Against the ‘gold’ standard, PICAR-Z exhibits a speed-up factor of roughly 152.4, 121.2, 203.9, and 177.4 for the count hurdle, semi-continuous hurdle, count mixture, and semi-continuous mixture models, respectively.

5 Applications

We demonstrate the scalability and flexibility of PICAR-Z on two large environmental datasets with spatially-referenced zero-inflated observations - zero-inflated counts of a bivalve species and high-resolution ice thickness measurement over West Antarctica.

5.1 Bivalve Species in the Dutch Wadden Sea

We examine a large spatial dataset of spatially-referenced bivalve species counts. The region of interest is the Dutch Wadden sea, a UNESCO site and a protected ecological habitat made up of sand barriers, salt marshes, mudflats, and gullies (Compton et al., 2013; Lyashevskaya et al., 2016). The Dutch Wadden sea is a famous stopover site for shorebirds (Lyashevskaya et al., 2016), particularly due to the presence of the Baltic tellin (*Macoma balthica*), a species of benthic invertebrates. Here, we examine spatial abundance data of the *Macoma balthica* species from Lyashevskaya et al. (2016) originally obtained from the synoptic intertidal benthic surveys (SIBES) monitoring program (Compton et al., 2013; Bijleveld et al., 2012). The observations consist of counts of the Baltic tellin (*Macoma balthica*) species sampled at $n = 4,029$ locations. Here, 65.9% of the locations have zero-counts. The occurrence (presence vs. absence) and prevalence (values of positive counts) maps are provided in the supplement.

We randomly select 3,220 observations to fit our model and hold out 806 observations for validation. Covariates include environmental variables that affect the abundance of the *Macoma balthica* species such as: (1) median grain size of the sediments; (2) silt content of the sediments; and (3) altitude. Using PICAR-Z, we fit the hurdle count model and the zero-inflated Poisson model (mixture). We construct a triangular mesh with $m = 4,028$ mesh vertices. In both the count hurdle and mixture cases, the automated heuristic (Section 3.3) chose ranks $p_o = 14$ and $p_p = 64$ for the occurrence and prevalence processes, respectively.

We employ similar model specifications and prior distributions as in the simulated ex-

amples (Section 4.2), including a comparisons to fixed-rank kriging. Comparative results are provided in the Table 7. Both the PICAR-Z and correlated PICAR-Z approach outperforms fixed rank kriging (bi-square basis functions) in predictions and shorter model-fitting walltimes. These results hold in both the hurdle and mixture modeling approaches. Note that PICAR-Z provides more accurate predictions, compared to fixed rank kriging, among the non-zero observations. Comparisons to the gold standard approach (Christensen and Waagepetersen, 2002) are computationally prohibitive due to the long wall times associated with the MCMC algorithms. Under PICAR-Z, both the hurdle and mixture models provide comparable out-of-sample predictions, yet the hurdle model has a shorter walltime; therefore, we recommend the count hurdle model for this particular case. We present the inferential results for the regression coefficients β_o and β_p in the supplement.

5.2 Ice-sheet Thickness Data for West Antarctica

Based on available geological records, mass loss from the Antarctic ice sheets can contribute considerable amounts to global sea level rise (Deschamps et al., 2012), in some cases up to 60 m (Fretwell et al., 2012). Nearly eight percent of the global population is threatened by five meter rise in sea level (Nicholls et al., 2008) and 13 percent of the global urban population is threatened by a ten meter sea level rise (McGranahan et al., 2007). An important first step entails modeling the current thickness of the Antarctic ice sheet at unobserved locations. We examine semicontinuous observations of ice thickness from the Bedmap2 dataset (Fretwell et al., 2012), generated using satellite altimetry, airborne and ground radar surveys, and seismic sounding. Similar to Chang et al. (2016), we examine gridded ice thickness observations at 20 km resolution over a 171×171 grid spanning the entirety of Antarctic. The resulting dataset consists of $n = 29,241$ semicontinuous observations of ice sheet thickness where 10,327 (35.3%) are zeros. However, the data is collected at regularly-spaced intervals with many unobserved locations in the spatial domain. To better understand the spatial structure of the Antarctic Ice sheet, we

aim to model the semicontinuous observations and interpolate at unknown locations.

We randomly select 23,000 locations to train our model, and reserve the remaining 6,241 locations for validation. We model the observed ice thickness data using: (1) a hurdle semicontinuous model with a lognormal prevalence process; and (2) a semi-continuous mixture model using the Tobit Type I model. We rescale the spatial domain into the unit square, and include the X- and Y- coordinates as covariates. We implement similar settings as the semi-continuous cases in Section 4 including the parameters' prior distributions. Due to the high-dimensional observations, we omit comparisons to the correlated PICAR-Z and 'gold standard' approaches. For PICAR-Z, we construct a triangular mesh with $m = 5,888$ mesh vertices. For both the hurdle model, the automated heuristic chose ranks $p_o = 46$ and $p_p = 200$ for the occurrence and prevalence processes, respectively. In the mixture model, we use ranks $p_o = 46$ and $p_p = 80$. For fixed rank kriging (bi-square basis functions), we use the quad-tree structure (84 basis functions) from Section 4.

Comparative results are provided in the Table 7 and maps of the predicted values are provided in Figure 7. Both PICAR-Z performs yields more accurate out-of-sample predictions than fixed rank kriging in both the total rmspe (hurdle: 353.31 vs. 372.53 and mixture: 314.47 vs. 323.77) and the rmspe among positive values (hurdle: 436.39 vs. 461.27 and mixture: 384.32 vs. 398.51). Both approaches yield comparable results among zero vs. non-zero predictions based on AUC (hurdle: 0.95 vs. 0.96 and mixture: 0.94 vs. 0.92). For the hurdle model, walltimes are slightly shorter for fixed rank kriging, which can be attributed to fewer basis functions chosen to represent the prevalence process. Despite the longer walltimes, PICAR-Z provides more accurate predictions and a larger effective sample size. The mixture model (Tobit Type I) is able to predict more accurately than the hurdle model; however, it comes at the cost of slightly longer walltimes.

6 Discussion

In this study, we propose a computationally efficient approach (PICAR-Z) to model high-dimensional zero-inflated spatial count and semi-continuous observations. Our method approximates the two latent spatial random fields using the PICAR representation. PICAR-Z scales well to higher dimensions, is automated, and extends to a wide range of spatial two-part models. In both simulated and real-world examples, PICAR-Z yields comparable results to the gold standard in both inference and prediction, yet incurs just a fraction of the computational costs. In addition, PICAR-Z outperforms a competing approach in both predictions and computational costs. Our method can be easily implemented in a programming language for Markov chain Monte Carlo algorithms such as `nimble` and `stan`. PICAR-Z significantly reduces computational overhead while maintaining model performance, thereby allowing practitioners to investigate a wider range of two-part spatial models than was previously possible.

While this study focuses on four types of two-part models, a natural extension would extend ideas from complex two-part models to the spatial context; examples include hurdle models with skewed distributions (Dreassi et al., 2014; Liu et al., 2016), t-distributions to model heavy tailed behavior (Neelon et al., 2015), or scale mixtures of normal distributions (Fruhworth-Schnatter and Pyne, 2010). Next, our approach does not provide a procedure for choosing between hurdle and mixture models, at least prior to model-fitting. Developing a formal test or automated heuristic to select the appropriate class of spatial two-part models would be a promising area of future research.

Extending PICAR-Z to the multivariate or spatio-temporal setting can be a promising direction for future research. The latent spatial processes can be linked using nonstationary multivariate covariance functions (Kleiber and Nychka, 2012) and or basis functions weighted with Gaussian graphical vectors (Krock et al., 2021). For spatio-temporal data, modeling basis coefficients as a vector-autoregressive process (Bradley et al., 2015) can induce temporal dependencies in the latent spatial occurrence and prevalence processes.

7 Acknowledgments

We are grateful to Yawen Guan and Jaewoo Park for helpful discussions. Any opinions, findings, and conclusions or recommendations expressed in this material are those of the authors and do not necessarily reflect the views of any funding entity. Any errors and opinions are, of course, those of the authors. We are not aware of any real or perceived conflicts of interest for any authors. Accompanying code can be accessed at the following github repository https://github.com/bene55/PICAR_Z_Code.

References

- Agarwal, D. K., Gelfand, A. E., and Citron-Pousty, S. (2002). Zero-inflated models with application to spatial count data. *Environmental and Ecological Statistics*, 9(4):341–355.
- Arcuti, S., Pollice, A., Ribocco, N., and D’Onghia, G. (2016). Bayesian spatiotemporal analysis of zero-inflated biological population density data by a delta-normal spatiotemporal additive model: Bayesian analysis of zero-inflated biological data. *Biometrical Journal*, 58(2):372–386.
- Banerjee, A., Dunson, D. B., and Tokdar, S. T. (2013). Efficient Gaussian process regression for large datasets. *Biometrika*, 100(1):75–89.
- Banerjee, S., Gelfand, A. E., Finley, A. O., and Sang, H. (2008). Gaussian predictive process models for large spatial data sets. *Journal of the Royal Statistical Society: Series B (Statistical Methodology)*, 70(4):825–848.
- Bijleveld, A. I., van Gils, J. A., van der Meer, J., Dekinga, A., Kraan, C., van der Veer, H. W., and Piersma, T. (2012). Designing a benthic monitoring programme with multiple conflicting objectives. *Methods in Ecology and Evolution*, 3(3):526–536.
- Bopp, G. P., Shaby, B. A., Forest, C. E., and Mejía, A. (2020). Projecting flood-inducing precipitation with a Bayesian analogue model. *Journal of Agricultural, Biological and Environmental Statistics*, 25(2):229–249.
- Bradley, J. R., Holan, S. H., and Wikle, C. K. (2019). Bayesian hierarchical models with conjugate full-conditional distributions for dependent data from the natural exponential family. *Journal of the American Statistical Association*, 0(ja):1–29.
- Bradley, J. R., Wikle, C. K., and Holan, S. H. (2015). Spatio-temporal change of support with application to American Community Survey multi-year period estimates. *Stat*, 4(1):255–270.

- Brenner, S. and Scott, R. (2007). *The Mathematical Theory of Finite Element Methods*, volume 15. Springer Science & Business Media.
- Chai, H. S. and Bailey, K. R. (2008). Use of log-skew-normal distribution in analysis of continuous data with a discrete component at zero. *Statistics in medicine*, 27(18):3643–3655.
- Chang, W., Haran, M., Applegate, P., and Pollard, D. (2016). Calibrating an ice sheet model using high-dimensional binary spatial data. *Journal of the American Statistical Association*, 111(513):57–72.
- Christensen, O. F., Roberts, G. O., and Sköld, M. (2006). Robust Markov chain Monte Carlo methods for spatial generalized linear mixed models. *Journal of Computational and Graphical Statistics*, 15(1):1–17.
- Christensen, O. F. and Waagepetersen, R. (2002). Bayesian prediction of spatial count data using generalized linear mixed models. *Biometrics*, 58(2):280–286.
- Compton, T. J., Holthuijsen, S., Koolhaas, A., Dekinga, A., ten Horn, J., Smith, J., Galama, Y., Brugge, M., van der Wal, D., van der Meer, J., et al. (2013). Distinctly variable mudscapes: Distribution gradients of intertidal macrofauna across the dutch wadden sea. *Journal of Sea Research*, 82:103–116.
- Cressie, N. and Johannesson, G. (2008). Fixed rank kriging for very large spatial data sets. *Journal of the Royal Statistical Society: Series B (Statistical Methodology)*, 70(1):209–226.
- Cressie, N. and Wikle, C. K. (2015). *Statistics for spatio-temporal data*. John Wiley & Sons.
- de Valpine, P., Turek, D., Paciorek, C., Anderson-Bergman, C., Temple Lang, D., and Bodik, R. (2017). Programming with models: writing statistical algorithms for general

- model structures with nimble. *Journal of Computational and Graphical Statistics*, 26:403–413.
- Deschamps, P., Durand, N., Bard, E., Hamelin, B., Camoin, G., Thomas, A. L., Henderson, G. M., Okuno, J., and Yokoyama, Y. (2012). Ice-sheet collapse and sea-level rise at the Bølling warming 14,600 years ago. *Nature*, 483(7391):559.
- Diggle, P. J., Tawn, J. A., and Moyeed, R. (1998). Model-based geostatistics. *Journal of the Royal Statistical Society: Series C (Applied Statistics)*, 47(3):299–350.
- Dreassi, E., Petrucci, A., and Rocco, E. (2014). Small area estimation for semicontinuous skewed spatial data: An application to the grape wine production in tuscany. *Biometrical Journal*, 56(1):141–156.
- Feng, C. X. (2021). A comparison of zero-inflated and hurdle models for modeling zero-inflated count data. *Journal of Statistical Distributions and Applications*, 8(1):1–19.
- Fernandes, M. V., Schmidt, A. M., and Migon, H. S. (2009). Modelling zero-inflated spatio-temporal processes. *Statistical Modelling: An International Journal*, 9(1):3–25.
- Fretwell, P., Pritchard, H., Vaughan, D., Bamber, J., Barrand, N., Bell, R., Bianchi, C., Bingham, R., Blankenship, D., Casassa, G., et al. (2012). Bedmap2: Improved ice bed, surface and thickness datasets for Antarctica. *The Cryosphere Discussions*, 6:4305–4361.
- Fruhworth-Schnatter, S. and Pyne, S. (2010). Bayesian inference for finite mixtures of univariate and multivariate skew-normal and skew-t distributions. *Biostatistics*, 11(2):317–336.
- Griffith, D. A. (2003). Spatial filtering. In *Spatial Autocorrelation and Spatial Filtering*, pages 91–130. Springer.
- Gschlößl, S. and Czado, C. (2008). Modelling count data with overdispersion and spatial effects. *Statistical Papers*, 49(3):531–552.

- Guan, Y. and Haran, M. (2018). A computationally efficient projection-based approach for spatial generalized linear mixed models. *Journal of Computational and Graphical Statistics*, 27(4):701–714.
- Guan, Y. and Haran, M. (2019). Fast expectation-maximization algorithms for spatial generalized linear mixed models. *arXiv preprint arXiv:1909.05440*.
- Guhaniyogi, R., Finley, A. O., Banerjee, S., and Gelfand, A. E. (2011). Adaptive Gaussian predictive process models for large spatial datasets. *Environmetrics*, 22(8):997–1007.
- Haran, M. (2011). Gaussian random field models for spatial data. *Handbook of Markov Chain Monte Carlo*, pages 449–478.
- Haran, M., Hodges, J. S., and Carlin, B. P. (2003). Accelerating computation in markov random field models for spatial data via structured MCMC. *Journal of Computational and Graphical Statistics*, 12(2):249–264.
- Higdon, D. (1998). A process-convolution approach to modelling temperatures in the North Atlantic Ocean. *Environmental and Ecological Statistics*, 5(2):173–190.
- Hjelle, Ø. and Dæhlen, M. (2006). *Triangulations and applications*. Springer Science & Business Media.
- Hughes, J. and Haran, M. (2013). Dimension reduction and alleviation of confounding for spatial generalized linear mixed models. *Journal of the Royal Statistical Society: Series B (Statistical Methodology)*, 75(1):139–159.
- Katzfuss, M. (2017). A multi-resolution approximation for massive spatial datasets. *Journal of the American Statistical Association*, 112(517):201–214.
- Kim, S. H., Chang, C.-C. H., Kim, K. H., Fine, M. J., and Stone, R. A. (2012). BLUP (REMQ) estimation of a correlated random effects negative binomial hurdle model. *Health Services and Outcomes Research Methodology*, 12(4):302–319.

- Kleiber, W. and Nychka, D. (2012). Nonstationary modeling for multivariate spatial processes. *Journal of Multivariate Analysis*, 112:76–91.
- Krock, M., Kleiber, W., Hammerling, D., and Becker, S. (2021). Modeling massive highly-multivariate nonstationary spatial data with the basis graphical lasso. *arXiv preprint arXiv:2101.02404*.
- Lambert, D. (1992). Zero-inflated Poisson regression, with an application to defects in manufacturing. *Technometrics*, 34(1):1–14.
- Lee, B. S. and Haran, M. (2021). PICAR: an efficient extendable approach for fitting hierarchical spatial models. *Technometrics*, pages 1–12.
- Lee, C.-E. and Kim, S. (2017). Applicability of zero-inflated models to fit the torrential rainfall count data with extra zeros in south korea. *Water*, 9(2):123.
- Lee, Y., Alam, M. M., Noh, M., Rönnegård, L., and Skarin, A. (2016). Spatial modeling of data with excessive zeros applied to reindeer pellet-group counts. *Ecology and evolution*, 6(19):7047–7056.
- Lehoucq, R. B., Sorensen, D. C., and Yang, C. (1998). *ARPACK users' guide: Solution of large-scale eigenvalue problems with implicitly restarted Arnoldi methods*, volume 6. Siam.
- Lindgren, F., Rue, H., et al. (2015). Bayesian spatial modelling with R-INLA. *Journal of Statistical Software*, 63(19):1–25.
- Lindgren, F., Rue, H., and Lindström, J. (2011). An explicit link between Gaussian fields and Gaussian Markov random fields: the stochastic partial differential equation approach. *Journal of the Royal Statistical Society: Series B (Statistical Methodology)*, 73(4):423–498.

- Liu, L., Strawderman, R. L., Johnson, B. A., and O'Quigley, J. M. (2016). Analyzing repeated measures semi-continuous data, with application to an alcohol dependence study. *Statistical Methods in Medical Research*, 25(1):133–152.
- Lyashevskaya, O., Brus, D. J., and van der Meer, J. (2016). Mapping species abundance by a spatial zero-inflated Poisson model: A case study in the Wadden Sea, the Netherlands. *Ecology and Evolution*, 6(2):532–543.
- McGranahan, G., Balk, D., and Anderson, B. (2007). The rising tide: Assessing the risks of climate change and human settlements in low elevation coastal zones. *Environment and Urbanization*, 19(1):17–37.
- Min, Y. and Agresti, A. (2005). Random effect models for repeated measures of zero-inflated count data. *Statistical modelling*, 5(1):1–19.
- Moran, P. A. (1950). Notes on continuous stochastic phenomena. *Biometrika*, 37(1/2):17–23.
- Moulton, L. H. and Halsey, N. A. (1995). A mixture model with detection limits for regression analyses of antibody response to vaccine. *Biometrics*, pages 1570–1578.
- Mullahy, J. (1986). Specification and testing of some modified count data models. *Journal of Econometrics*, 33(3):341–365.
- Neelon, B. (2019). Bayesian zero-inflated negative binomial regression based on Pólya-gamma mixtures. *Bayesian Analysis*, 14(3):829.
- Neelon, B., Chang, H. H., Ling, Q., and Hastings, N. S. (2016a). Spatiotemporal hurdle models for zero-inflated count data: Exploring trends in emergency department visits. *Statistical Methods in Medical Research*, 25(6):2558–2576.
- Neelon, B., O'Malley, A. J., and Smith, V. A. (2016b). Modeling zero-modified count and semicontinuous data in health services research Part 1: Background and overview. *Statistics in Medicine*, 35(27):5070–5093.

- Neelon, B., O'Malley, A. J., and Normand, S.-L. T. (2011). A Bayesian two-part latent class model for longitudinal medical expenditure data: Assessing the impact of mental health and substance abuse parity. *Biometrics*, 67(1):280–289.
- Neelon, B., Zhu, L., and Neelon, S. E. B. (2015). Bayesian two-part spatial models for semicontinuous data with application to emergency department expenditures. *Biostatistics*, 16(3):465–479.
- Nicholls, R. J., Tol, R. S., and Vafeidis, A. T. (2008). Global estimates of the impact of a collapse of the West Antarctic ice sheet: An application of FUND. *Climatic Change*, 91(1-2):171.
- Nychka, D., Bandyopadhyay, S., Hammerling, D., Lindgren, F., and Sain, S. (2015). A multiresolution Gaussian process model for the analysis of large spatial datasets. *Journal of Computational and Graphical Statistics*, 24(2):579–599.
- Oliver, D. S. (2003). Gaussian cosimulation: modelling of the cross-covariance. *Mathematical Geology*, 35(6):681–698.
- Olsen, M. K. and Schafer, J. L. (2001). A two-part random-effects model for semicontinuous longitudinal data. *Journal of the American Statistical Association*, 96(454):730–745.
- Park, J. and Haran, M. (2020). Reduced-dimensional Monte Carlo maximum likelihood for latent Gaussian random field models. *Journal of Computational and Graphical Statistics*, 30(2):269–283.
- Qiu, Y. and Mei, J. (2019). *RSpectra: Solvers for Large-Scale Eigenvalue and SVD Problems*. R package version 0.15-0.
- Rasmussen, C. and Williams, C. (2006). *Gaussian Processes for Machine Learning*. Adaptive Computation and Machine Learning. MIT Press, Cambridge, MA, USA.

- Rasmussen, C. E. (2004). Gaussian processes in machine learning. In *Advanced Lectures on Machine Learning*, pages 63–71. Springer.
- Rathbun, S. L. and Fei, S. (2006). A spatial zero-inflated poisson regression model for oak regeneration. *Environmental and Ecological Statistics*, 13(4):409–426.
- Recta, V., Haran, M., and Rosenberger, J. L. (2012). A two-stage model for incidence and prevalence in point-level spatial count data. *Environmetrics*, 23(2):162–174.
- Roeder, K., Lynch, K. G., and Nagin, D. S. (1999). Modeling uncertainty in latent class membership: A case study in criminology. *Journal of the American Statistical Association*, 94(447):766–776.
- Rue, H., Martino, S., and Chopin, N. (2009). Approximate Bayesian inference for latent Gaussian models by using integrated nested Laplace approximations. *Journal of the Royal Statistical Society: Series B (Statistical Methodology)*, 71(2):319–392.
- Sengupta, A. and Cressie, N. (2013). Hierarchical statistical modeling of big spatial datasets using the exponential family of distributions. *Spatial Statistics*, 4:14–44.
- Stein, M. L. (2012). *Interpolation of Spatial Data: Some Theory for Kriging*. Springer Science & Business Media.
- Tobin, J. (1958). Estimation of relationships for limited dependent variables. *Econometrica: Journal of the Econometric Society*, pages 24–36.
- Ver Hoef, J. M. and Jansen, J. K. (2007). Space—time zero-inflated count models of harbor seals. *Environmetrics*, 18(7):697–712.
- Vuong, Q. H. (1989). Likelihood ratio tests for model selection and non-nested hypotheses. *Econometrica: Journal of the Econometric Society*, pages 307–333.
- Wang, X., Chen, M.-H., Kuo, R. C., and Dey, D. K. (2015). Bayesian spatial-temporal modeling of ecological zero-inflated count data. *Statistica Sinica*, 25(1):189.

List of Figures

1	Prediction results from a single simulated example. Data are generated from the spatial count mixture model in Section 4. Top row includes the true and predicted probability surfaces $\pi(\mathbf{s})$ for the occurrence random process $O(\mathbf{s})$. Bottom row presents the true and predicted log-intensity surfaces $\log(\theta(\mathbf{s}))$ for the prevalence random process $P(\mathbf{s})$. Column 1 presents the true latent probability and log-intensity surfaces. Columns 2-3 include the predicted surfaces for PICAR-Z (column 2), fixed rank kriging with bi-square basis functions (column 3), and the ‘gold standard’ approach (column 4). In the fifth column, a color scale is provided for the probability and log-intensity surfaces.	36
2	Maps of the observed ice-thickness at the 6,241 validation locations (top left). Predicted values using the hurdle semi-continuous model with PICAR-Z (top middle) and fixed rank kriging (top right). Predictions using the mixture semi-continuous model with PICAR-Z (bottom middle) and fixed rank kriging (bottom right).	37

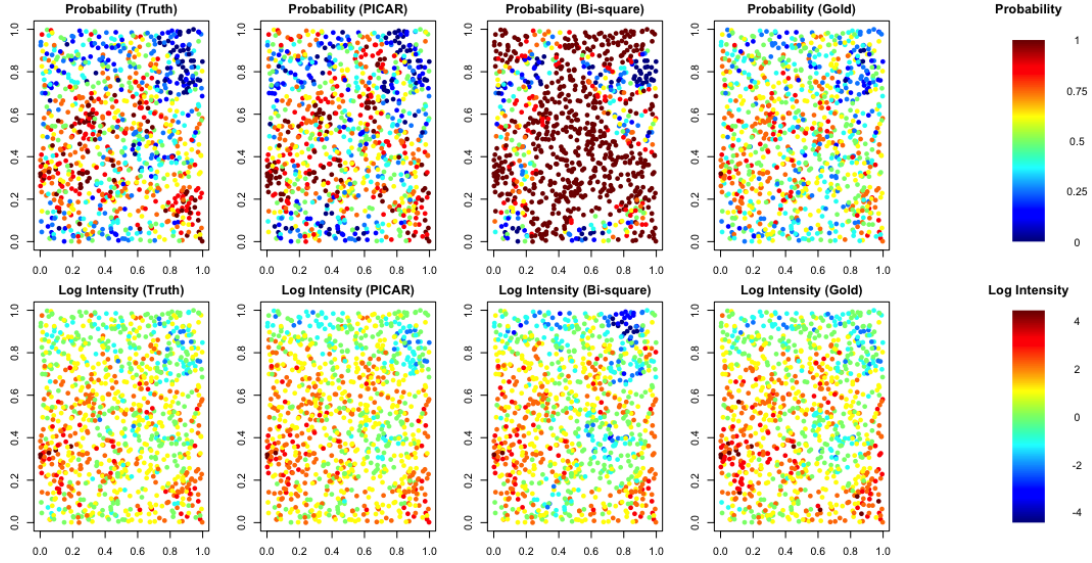


Figure 1: Prediction results from a single simulated example. Data are generated from the spatial count mixture model in Section 4. Top row includes the true and predicted probability surfaces $\pi(\mathbf{s})$ for the occurrence random process $O(\mathbf{s})$. Bottom row presents the true and predicted log-intensity surfaces $\log(\theta(\mathbf{s}))$ for the prevalence random process $P(\mathbf{s})$. Column 1 presents the true latent probability and log-intensity surfaces. Columns 2-3 include the predicted surfaces for PICAR-Z (column 2), fixed rank kriging with bi-square basis functions (column 3), and the ‘gold standard’ approach (column 4). In the fifth column, a color scale is provided for the probability and log-intensity surfaces.

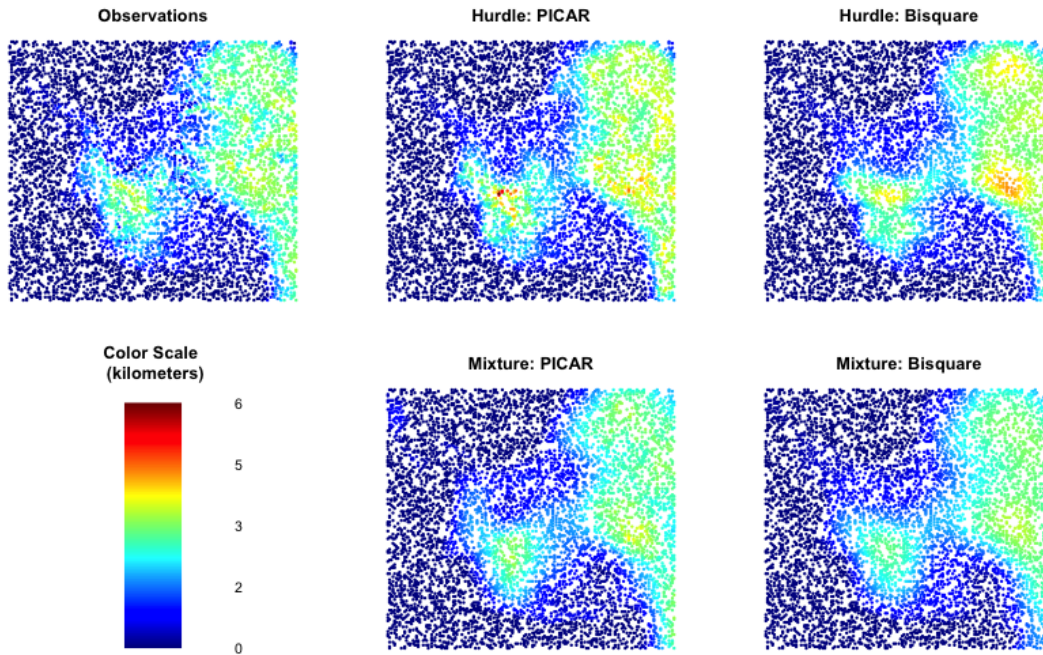


Figure 2: Maps of the observed ice-thickness at the 6,241 validation locations (top left). Predicted values using the hurdle semi-continuous model with PICAR-Z (top middle) and fixed rank kriging (top right). Predictions using the mixture semi-continuous model with PICAR-Z (bottom middle) and fixed rank kriging (bottom right).

List of Tables

1	Summary of Spatial Two-part Models	39
2	Summary of Common Spatial Two-part models. Models are broken down by class (hurdle vs. mixture) and data type (discrete vs. semi-continuous).	39
3	Simulation Study Results: Median values for all 100 samples in the simulation study. Results are grouped by two-part model (hurdle vs. mixture), data type (counts vs. semi-continuous), and approach (PICAR-Z, PICAR-Z with cross-correlation, fixed rank kriging using bi-square basis functions, and the gold standard). Results include the root mean squared prediction error (rmspe) for the entire validation dataset and the non-zero data. For zero- vs. non-zero classification, we report the area under the ROC curve (AUC). Model-fitting walltimes are reported in minutes.	40
4	Bivalve Species Results: Results are grouped by two-part model (hurdle vs. mixture) and approach (PICAR-Z, PICAR-Z with cross-correlation, and fixed rank kriging using bi-square basis functions). Results include the root mean squared prediction error (rmspe) for the entire validation dataset and the non-zero data. For zero- vs. non-zero classification, we report the area under the ROC curve (AUC). Model-fitting walltimes are reported in minutes.	41
5	West Antarctica Ice Thickness Results: Results are grouped by two-part model (hurdle vs. mixture) and approach (PICAR-Z vs. fixed rank kriging using bi-square basis functions). Results include the root mean squared prediction error (rmspe) for the entire validation dataset and the non-zero data. For zero- vs. non-zero classification, we report the area under the ROC curve (AUC). Model-fitting walltimes are reported in minutes. . . .	42

Table 1: Summary of Spatial Two-part Models

Class	Data Type	Occurrence $O(s)$	Prevalence $P(s)$
Hurdle	Discrete	Bernouilli Bernouilli	Zero-Truncated Poisson Zero-Truncated Neg. Binomial
	Continuous	Bernouilli Bernouilli	Lognormal Log skew-normal
Mixture	Discrete	Bernouilli Bernouilli	Poisson Negative Binomial
	Continuous	Bernouilli	Tobit Type I Model

Table 2: Summary of Common Spatial Two-part models. Models are broken down by class (hurdle vs. mixture) and data type (discrete vs. semi-continuous).

Two-Part Model	Fitting Method	Total RMSPE	Non-Zero RMSPE	Zero AUC	Time (mins)
Count Hurdle	PICAR-Z	2.182	2.594	0.726	1.500
	PICAR-Z (Cor)	2.195	2.581	0.725	2.100
	Bi-square	2.252	2.701	0.722	2.200
	Gold Standard	2.209	2.952	0.723	228.600
Semi-continuous Hurdle	PICAR-Z	2.376	2.917	0.737	1.900
	PICAR-Z (Cor)	2.353	2.953	0.736	3.500
	Bi-square	2.834	3.503	0.731	2.200
	Gold Standard	2.532	3.285	0.734	230.300
Count Mixture	PICAR-Z	2.366	3.374	0.805	1.900
	PICAR-Z (Cor)	2.366	3.364	0.806	2.600
	Bi-square	2.528	3.462	0.802	2.700
	Gold Standard	2.428	3.704	0.806	387.400
Semi-continuous Mixture	PICAR-Z	0.515	0.825	0.854	2.200
	PICAR-Z (Cor)	0.518	0.831	0.859	3.200
	Bi-square	0.563	0.882	0.789	2.700
	Gold Standard	0.676	1.081	0.734	390.200

Table 3: Simulation Study Results: Median values for all 100 samples in the simulation study. Results are grouped by two-part model (hurdle vs. mixture), data type (counts vs. semi-continuous), and approach (PICAR-Z, PICAR-Z with cross-correlation, fixed rank kriging using bi-square basis functions, and the gold standard). Results include the root mean squared prediction error (rmspe) for the entire validation dataset and the non-zero data. For zero- vs. non-zero classification, we report the area under the ROC curve (AUC). Model-fitting walltimes are reported in minutes.

Two-Part Model	Fitting Method	Total RMSPE	Non-Zero RMSPE	Zero AUC	Time (mins)
Count Hurdle	PICAR-Z	4.50	7.41	0.64	2.53
	PICAR-Z (Cor)	4.50	7.40	0.64	3.05
	Bi-square	4.80	7.83	0.64	3.15
Count Mixture	PICAR-Z	4.51	7.41	0.64	4.53
	PICAR-Z (Cor)	4.52	7.41	0.64	4.88
	Bi-square	4.82	7.89	0.64	4.95

Table 4: Bivalve Species Results: Results are grouped by two-part model (hurdle vs. mixture) and approach (PICAR-Z, PICAR-Z with cross-correlation, and fixed rank kriging using bi-square basis functions). Results include the root mean squared prediction error (rmspe) for the entire validation dataset and the non-zero data. For zero- vs. non-zero classification, we report the area under the ROC curve (AUC). Model-fitting walltimes are reported in minutes.

Two-Part Model	Fitting Method	Total RMSPE	Non-Zero RMSPE	Zero AUC	Time (mins)
Semi-Continuous Hurdle	PICAR-Z	352.31	436.39	0.95	31.47
	Bi-square	372.53	461.27	0.96	28.73
Semi-Continuous Mixture	PICAR-Z	314.47	384.32	0.94	33.44
	Bi-square	323.77	398.51	0.92	34.29

Table 5: West Antarctica Ice Thickness Results: Results are grouped by two-part model (hurdle vs. mixture) and approach (PICAR-Z vs. fixed rank kriging using bi-square basis functions). Results include the root mean squared prediction error (rmspe) for the entire validation dataset and the non-zero data. For zero- vs. non-zero classification, we report the area under the ROC curve (AUC). Model-fitting walltimes are reported in minutes.

Supplement: A Class of Models for Large Zero-inflated Spatial Data

Ben Seiyon Lee*

Department of Statistics, George Mason University

Murali Haran

Department of Statistics, The Pennsylvania State University

1 Two-Part Models for Zero-inflated Data

In this section, we review the two-part modeling framework (Mullahy, 1986; Lambert, 1992) for zero-inflated data. Two-part models are comprised of two random variables: (1) the occurrence random variable O that generates the structural zero and non-zeros cases; and (2) the prevalence random variable P , which assigns positive values for the structural non-zero cases. In special cases, the prevalence random variable P can also generate zeros. In two-part models, the zero-inflated observation Z is generated as follows:

$$Z = \begin{cases} 0 & \text{if } O = 0 \\ P & \text{if } O = 1. \end{cases}, \quad (1)$$

where O and P are the latent occurrence and prevalence random variables, respectively. The occurrence variable $O \in \{0, 1\}$ is typically modeled as a Bernoulli random variable with probability $\pi \in (0, 1)$ (i.e., $O \sim \text{Bern}(\pi)$). The prevalence variable is distributed as

*Corresponding Author: Department of Statistics, George Mason University; 4400 University Drive, MS 4A7; Fairfax, VA 22030-4444; United States of America (e-mail: slee287@gmu.edu)

$P \sim F(\boldsymbol{\theta})$ where $F(\boldsymbol{\theta})$ is a discrete probability mass function or continuous probability density function with prevalence model parameter $\boldsymbol{\theta}$.

Two-part models for zero-inflated data typically fall into two classes - hurdle and mixture models. In *hurdle models*, the occurrence random variable specifies which data have zero- or non-zero values. For the non-zero data, their respective positive values are generated via the prevalence random variable P . In the discrete case, $F(\cdot)$ is a zero-truncated probability mass function such as the zero-truncated Poisson or the zero-truncated negative binomial distribution. For semi-continuous observations, $F(\cdot)$ is a probability density function with positive support such as a log-normal or gamma distribution. For *mixture models*, the zero-valued observations can be generated by both the occurrence O and prevalence random variables P . Here, O determines whether a data point is classified as a structural zero or structural non-zero case. For the structural non-zero cases, the prevalence random variable P can generate both zeros and positive values. In the discrete case, $F(\cdot)$ is a non-degenerate mass function such as the Poisson or Negative-Binomial distribution. For semi-continuous observations, $f(\cdot)$ can be a censored model such as a Tobit Type I.

The probability mass (or density) function $f_Z(z)$ for two-part models is as follows:

$$f_Z(z) = \begin{cases} (1 - \pi) + \pi\tilde{f}(0), & \text{if } z = 0 \\ \pi\tilde{f}(z), & \text{if } z > 0. \end{cases}, \quad (2)$$

where $\pi \in (0, 1)$ is occurrence probability, $\tilde{f}(z)$ is a probability mass or density function for the prevalence random variable with parameters $\boldsymbol{\theta}$. For two part models, the expectation is defined as $E[Z|\pi, \boldsymbol{\theta}] = \pi E_{\tilde{f}}[Z|\boldsymbol{\theta}]$ and the variance is $Var[Z|\pi, \boldsymbol{\theta}] = \pi(1 - \pi)E_{\tilde{f}}[Z|\boldsymbol{\theta}]^2 + \pi Var_{\tilde{f}}[Z|\boldsymbol{\theta}]$ where $E_{\tilde{f}}[Z|\boldsymbol{\theta}]$ and $Var_{\tilde{f}}[Z|\boldsymbol{\theta}]$ denote the expectation and variance of a random variable with probability mass or density function $\tilde{f}(\cdot)$ and parameter $\boldsymbol{\theta}$.

Alternative distributions of $\tilde{F}(\cdot)$ can result in richer and more flexible two-part models. For count data, examples include the Poisson, negative binomial, zero-truncated Poisson

(Lambert, 1992), translated Poisson (Ver Hoef and Jansen, 2007), zero-truncated negative binomial (?), generalized Poisson (Gschlößl and Czado, 2008), and binomial distributions (?). In the semi-continuous case, the lognormal distribution may not be appropriate due to the lack of symmetry or fatter tails exhibited by the observations. Past studies have used skewed distributions (Dreassi et al., 2014; Liu et al., 2016), t-distributions to model heavy tailed behavior (Neelon et al., 2015), or modeled the prevalence process using scale mixtures of normal distributions (Fruhirth-Schnatter and Pyne, 2010).

Since two-part models have a natural hierarchical structure (Equation 1), they can be readily incorporated into the Bayesian hierarchical modeling framework. The general Bayesian hierarchical model is as follows:

Data Model:	$Z O, P \sim F(\cdot O, P)$
Process Model:	$O \pi \sim \text{Bern}(\pi)$
	$P \theta \sim \tilde{F}(\theta)$
Parameter Model:	Priors for π and θ

1.1 Spatial Generalized Linear Mixed Models

In the literature, the spatially-dependent occurrence $O(\mathbf{s})$ and prevalence $P(\mathbf{s})$ processes have been modeled as spatial generalized linear mixed models (SGLMMs)(cf. Agarwal et al., 2002; Rathbun and Fei, 2006; ?; Recta et al., 2012). Spatial generalized linear mixed models are a popular choice for modeling spatial data (Diggle et al., 1998; Haran, 2011), particularly non-Gaussian data. Let $\{Z(\mathbf{s}) : \mathbf{s} \in \mathcal{D}\}$ be a non-Gaussian spatial random process. Assuming the realizations $Z(\mathbf{s})$ are conditionally independent given the latent spatial random effects $W(\mathbf{s})$, the conditional mean $E[Z(\mathbf{s})|\boldsymbol{\beta}, W(\mathbf{s}), \epsilon(\mathbf{s})]$ can be modeled through the linear predictor $\eta(\mathbf{s})$:

$$\eta(\mathbf{s}) = g\{E[Z(\mathbf{s})|\boldsymbol{\beta}, W(\mathbf{s}), \epsilon(\mathbf{s})]\} = \mathbf{X}(\mathbf{s})'\boldsymbol{\beta} + W(\mathbf{s}) + \epsilon(\mathbf{s}),$$

where $g(\cdot)$ is a known link function and $\epsilon(\mathbf{s})$ is micro-scale measurement error typically modeled as an uncorrelated Gaussian process where $\epsilon(\mathbf{s}) \sim N(0, \tau^2)$ for $\mathbf{s} \in \mathcal{D}$. Binary and count observations are two common types of non-Gaussian spatial data, and these can be modeled using the binary SGLMM with logit link and the Poisson SGLMM with log link, respectively. The general Bayesian hierarchical framework for the SGLMM is:

$$\begin{aligned}
\text{Data Model:} \quad & Z(\mathbf{s})|\mu(\mathbf{s}) \sim F(\cdot | \mu(\mathbf{s})), \quad \mu(\mathbf{s}) = \mathbb{E}[Z(\mathbf{s})|\boldsymbol{\beta}, W(\mathbf{s}), \epsilon(\mathbf{s})] \\
& \eta(\mathbf{s}) = g(\mu(\mathbf{s})) = \mathbf{X}(\mathbf{s})'\boldsymbol{\beta} + W(\mathbf{s}) + \epsilon(\mathbf{s}) \\
\text{Process Model:} \quad & \mathbf{W}|\boldsymbol{\Theta} \sim N(\mathbf{0}, \mathbf{C}(\boldsymbol{\Theta})), \quad \mathbf{W} = (W(\mathbf{s}_1), \dots, W(\mathbf{s}_n))' \\
& \epsilon(\mathbf{s})|\tau^2 \sim \mathcal{N}(0, \tau^2) \\
\text{Parameter Model:} \quad & \boldsymbol{\beta} \sim p(\boldsymbol{\beta}), \quad \boldsymbol{\Theta} \sim p(\boldsymbol{\Theta}), \quad \tau^2 \sim p(\tau^2)
\end{aligned}$$

where $F(\cdot | \mu(\mathbf{s}))$ is a probability distribution (e.g. Bernoulli or Poisson), $\boldsymbol{\beta}$ and $\mathbf{X}(\mathbf{s})$ are the k -dimensional vector of the fixed effects and covariates for location \mathbf{s}_i , respectively. \mathbf{W} is the n -dimensional vector of the spatial random effects, and τ^2 is the nugget variance. $\mathbf{C}(\boldsymbol{\Theta})$ is the covariance matrix for the spatial random effects \mathbf{W} with covariance parameter $\boldsymbol{\Theta}$.

To account for spatial dependence, $\mathbf{W} = \{W(\mathbf{s}) : \mathbf{s} \in \mathcal{D}\}$ can be modeled as a stationary zero-mean Gaussian process with a positive definite covariance function $C(\cdot)$. For a finite set of locations, the spatial random effects \mathbf{W} follow a multivariate normal distribution $\mathbf{W}|\boldsymbol{\Theta} \sim N(\mathbf{0}, \mathbf{C}(\boldsymbol{\Theta}))$ with covariance matrix $\mathbf{C}(\boldsymbol{\Theta})$ defined such that $\mathbf{C}(\boldsymbol{\Theta})_{ij} = \text{Cov}(W(\mathbf{s}_i), W(\mathbf{s}_j))$ and covariance function parameter $\boldsymbol{\Theta}$. The Matérn covariance function is a widely used class of stationary and isotropic covariance functions (Stein, 2012) defined as:

$$\mathbf{C}(\mathbf{s}_i, \mathbf{s}_j) = \sigma^2 \frac{1}{\Gamma(\nu)2^{\nu-1}} \left(\sqrt{2\nu} \frac{h}{\phi} \right)^\nu K_\nu \left(\sqrt{2\nu} \frac{h}{\phi} \right) \quad (3)$$

where $h = \|\mathbf{s}_i - \mathbf{s}_j\|$ is the Euclidean distance between locations \mathbf{s}_i and \mathbf{s}_j , $\sigma^2 > 0$ is

the partial sill or scale parameter of the process, and $\phi > 0$ is the range parameter for spatial dependence. $K_\nu(\cdot)$ is the modified Bessel function of the second kind where the smoothness parameter ν is commonly fixed prior to model fitting.

2 Competing Approaches

In both the simulation studies, we compare the PICAR-Z approach to two competing methods, fixed rank kriging (Cressie and Johannesson, 2008; Sengupta and Cressie, 2013) and a ‘gold standard’ method based on reparameterizing the spatial random effects (Christensen and Waagepetersen, 2002). We provide a brief overview and implementation details specific to our study.

2.1 Fixed Rank Kriging

We employ the bisquare basis function with a quad-tree structure from Sengupta and Cressie (2013). We use a hierarchical structure of bisquare basis functions centered at fixed knot locations. Let $\Phi_{\mathbf{c}_i}(\mathbf{s})$ denote the bisquare basis function centered at knot location \mathbf{c}_i with support on $\mathbf{s} \in \mathcal{D}$, the spatial domain. The general form of the bisquare basis function is:

$$\Phi_{\mathbf{c}_i}(\mathbf{s}) = \left\{ 1 - \left(\frac{\|\mathbf{s} - \mathbf{c}_i\|}{\omega} \right)^2 \right\}^2 I(\|\mathbf{s} - \mathbf{c}_i\| < \omega),$$

where \mathbf{s} is an observation location and \mathbf{c}_i is the i -th knot location (i.e. center of the basis function). The bi-square basis functions have locally bounded support $\{\mathbf{s} \in \mathbb{R}^2 : \|\mathbf{s} - \mathbf{c}_i\| < \omega\}$ that is controlled by the ‘aperture’, or threshold, $\omega > 0$.

As in past studies (cf. Sengupta and Cressie, 2013; ?; ?), we employ the quad-tree structure to select the centers (knots) of the bisquare basis functions; thereby ensuring that the knots for different resolutions do not overlap. Moreover, we placed knots outside the observed spatial domain ? to account for boundary effects. In this study, we use three

resolutions $J = 3$, where there are four knot locations $\mathbf{c}_1, \dots, \mathbf{c}_4$ for the first resolution, 16 knots $\mathbf{c}_5, \dots, \mathbf{c}_{20}$ for the second resolution, and 64 knots $\mathbf{c}_{21}, \dots, \mathbf{c}_{84}$ for the third resolution. The resolution-specific ‘‘apertures’’ (thresholds) ω_j for $j = 1, \dots, J$ are defined to be 1.5 times the shortest distance between like-resolution knot locations. We constructed a set of 84 bisquare basis functions $\Phi_{\mathbf{c}_i}(\mathbf{s})$ for $\mathbf{c}_i \in \mathbf{c}_1, \dots, \mathbf{c}_{84}$ allocated proportionally across the three resolutions.

We can embed the multi-resolution bisquare basis functions into the Bayesian hierarchical framework for spatial two-part models as follows:

$$\begin{aligned}
\text{Data Model:} & \quad Z(\mathbf{s})|O(\mathbf{s}), P(\mathbf{s}) \sim F(\cdot | O(\mathbf{s}), P(\mathbf{s})) \\
\text{Process Model:} & \quad O(\mathbf{s})|\pi(\mathbf{s}) \sim \text{Bern}(\pi(\mathbf{s})) \\
& \quad P(\mathbf{s})|\boldsymbol{\theta}(\mathbf{s}) \sim \tilde{F}(\cdot | \boldsymbol{\theta}(\mathbf{s})) \\
\text{Sub-process Model 1:} & \quad \pi(\mathbf{s})|\eta_o(\mathbf{s}) = g_o^{-1}(\eta_o(\mathbf{s})) \\
\text{(Occurrence)} & \quad \eta_o(\mathbf{s})|\boldsymbol{\beta}_o, \boldsymbol{\delta}_o(\mathbf{s}) = \mathbf{X}(\mathbf{s})'\boldsymbol{\beta}_o + \Phi(\mathbf{s})'\boldsymbol{\delta}_o(\mathbf{s}) \\
& \quad \boldsymbol{\delta}_o|\tau_o^2 \sim \mathcal{N}(\mathbf{0}, \tau_o^2 \boldsymbol{\Sigma}_o) \\
\text{Sub-process Model 2:} & \quad \theta(\mathbf{s})|\eta_p(\mathbf{s}) = g_p^{-1}(\eta_p(\mathbf{s})) \\
\text{(Prevalence)} & \quad \eta_p(\mathbf{s})|\boldsymbol{\beta}_p, \boldsymbol{\delta}_p(\mathbf{s}) = \mathbf{X}(\mathbf{s})'\boldsymbol{\beta}_p + \Phi(\mathbf{s})'\boldsymbol{\delta}_p(\mathbf{s}) \\
& \quad \boldsymbol{\delta}_p|\tau_p^2 \sim \mathcal{N}(\mathbf{0}, \tau_p^2 \boldsymbol{\Sigma}_p) \\
\text{Parameter Model:} & \quad \boldsymbol{\beta}_o \sim \mathcal{N}(\boldsymbol{\mu}_{\beta_o}, \boldsymbol{\Sigma}_{\beta_o}), \quad \boldsymbol{\beta}_p \sim \mathcal{N}(\boldsymbol{\mu}_{\beta_p}, \boldsymbol{\Sigma}_{\beta_p}) \\
& \quad \tau_o^2 \sim \mathcal{IG}(\alpha_{\tau_o}, \beta_{\tau_o}), \quad \tau_p^2 \sim \mathcal{IG}(\alpha_{\tau_p}, \beta_{\tau_p})
\end{aligned}$$

where Φ denotes the matrix of the multi-resolution bi-square basis functions defined as:

$$\Phi = \begin{bmatrix} \Phi_{\mathbf{c}_1} & \Phi_{\mathbf{c}_2} & \cdots & \Phi_{\mathbf{c}_{84}} \end{bmatrix}$$

In this study, we implement the three-resolution structure with 84 total basis functions. The hierarchical model is completed by assigning prior distributions for the model param-

eters β_o , β_p , σ_o^2 and σ_p^2 . In the simulation study, we use the following prior distributions for the model parameters, $\beta_o \sim \mathcal{N}(\mathbf{0}, 100\mathbf{I})$, $\beta_p \sim \mathcal{N}(\mathbf{0}, 100\mathbf{I})$, $\tau_o^2 \sim \mathcal{IG}(0.002, 0.002)$, and $\tau_p^2 \sim \mathcal{IG}(0.002, 0.002)$

2.2 Reparameterization

Reparameterization approaches (Christensen and Waagepetersen, 2002; Haran et al., 2003; Guan and Haran, 2018) have been designed to reduce correlation in the spatial random effects, which often results in faster mixing MCMC algorithms. However, these techniques can be very expensive for high-dimensional data, since the reparameterization step still requires an expensive Cholesky decomposition $\mathcal{O}(n^3)$ and the number of spatial random effects remain unchanged.

We employ a the reparameterization approach from Christensen and Waagepetersen (2002) where the latent spatial processes are reparameterized as $\mathbf{W}_o = \mathbf{L}_o\gamma_o$ and $\mathbf{W}_p = \mathbf{L}_p\gamma_p$ where \mathbf{L}_o and \mathbf{L}_p are the lower triangular matrices obtained through the Cholesky decomposition of the corresponding covariance matrices (i.e., $C_o(h; \sigma_o^2, \phi_o) = \mathbf{L}_o\mathbf{L}_o'$ and $C_p(h; \sigma_p^2, \phi_p) = \mathbf{L}_p\mathbf{L}_p'$). For strongly correlated spatial random effects, this approach results in approximately independent reparameterized spatial random effects γ_o and γ_p for the occurrence and prevalence processes, respectively; thereby improving mixing in MCMC algorithms (Christensen and Waagepetersen, 2002; Christensen et al., 2006).

Under the reparameterization framework, the Bayesian hierarchical model for spatial

two-part models is:

$$\begin{aligned}
\text{Data Model:} & \quad \mathbf{Z}|O(\mathbf{s}), P(\mathbf{s}) \sim F(\cdot | O(\mathbf{s}), P(\mathbf{s})) & (4) \\
\text{Process Model:} & \quad O(\mathbf{s})|\pi(\mathbf{s}) \sim \text{Bern}(\cdot|\pi(\mathbf{s})) \\
& \quad P(\mathbf{s})|\boldsymbol{\theta}(\mathbf{s}) \sim \tilde{F}(\cdot|\boldsymbol{\theta}(\mathbf{s})) \\
\text{Sub-process Model 1:} & \quad \pi(\mathbf{s})|\eta_o(\mathbf{s}) = g_o^{-1}(\eta_o(\mathbf{s})) \\
\text{(Occurrence)} & \quad \eta_o(\mathbf{s})|\boldsymbol{\beta}_o, \boldsymbol{\gamma}_o = \mathbf{X}(\mathbf{s})'\boldsymbol{\beta}_o + [\mathbf{L}_{\phi_o}\boldsymbol{\gamma}_o](\mathbf{s}) \\
& \quad \mathbf{R}_{\phi_o} = \mathbf{L}_{\phi_o}\mathbf{L}'_{\phi_o} \\
& \quad \boldsymbol{\gamma}_o|\sigma_o^2 \sim \mathcal{N}(\mathbf{0}, \sigma_o^2\mathbf{I}), \\
\text{Sub-process Model 2:} & \quad \theta(\mathbf{s})|\eta_p(\mathbf{s}) = g_p^{-1}(\eta_p(\mathbf{s})) \\
\text{(Prevalence)} & \quad \eta_p(\mathbf{s})|\boldsymbol{\beta}_p, \boldsymbol{\gamma}_p = \mathbf{X}(\mathbf{s})\boldsymbol{\beta}_p + [\mathbf{L}_{\phi_p}\boldsymbol{\gamma}_p](\mathbf{s}) \\
& \quad \mathbf{R}_{\phi_p} = \mathbf{L}_{\phi_p}\mathbf{L}'_{\phi_p} \\
& \quad \boldsymbol{\gamma}_p|\sigma_p^2 \sim \mathcal{N}(\mathbf{0}, \sigma_p^2\mathbf{I}), \\
\text{Parameter Model:} & \quad \boldsymbol{\beta}_o \sim p(\boldsymbol{\beta}_o), \quad \boldsymbol{\beta}_p \sim p(\boldsymbol{\beta}_p), \quad \phi_o \sim p(\phi_o), \quad \phi_p \sim p(\phi_p) \\
& \quad \sigma_o^2 \sim p(\sigma_o^2), \quad \sigma_p^2 \sim p(\sigma_p^2) & (5)
\end{aligned}$$

where $F(\cdot | O(\mathbf{s}), P(\mathbf{s}))$ is the distribution function of a spatial two-part model. \mathbf{R}_{ϕ_o} and \mathbf{R}_{ϕ_p} are the correlation matrices for the spatial occurrence and prevalence processes, respectively. For this approach, we assume that the class of the Matérn correlation function is known ($\nu = 0.5$). ϕ_o and ϕ_p denote the range parameters for the occurrence and prevalence cases. A Cholesky decomposition of \mathbf{R}_{ϕ_o} and \mathbf{R}_{ϕ_p} result in lower triangular matrices \mathbf{L}_{ϕ_o} and \mathbf{L}_{ϕ_p} .

In the simulation study, we use the following prior distributions for the model parameters, $\boldsymbol{\beta}_o \sim \mathcal{N}(\mathbf{0}, 100\mathbf{I})$, $\boldsymbol{\beta}_p \sim \mathcal{N}(\mathbf{0}, 100\mathbf{I})$, $\phi_o \sim \mathcal{U}(0, \sqrt{2})$, $\phi_p \sim \mathcal{U}(0, \sqrt{2})$, $\sigma_o^2 \sim \mathcal{IG}(0.002, 0.002)$, and $\sigma_p^2 \sim \mathcal{IG}(0.002, 0.002)$

	PICAR-Z	Correlated PICAR-Z	Fixed Rank Kriging	Gold Standard
Count Hurdle	100.0	74.9	49.4	0.7
Semi-continuous Hurdle	79.3	52.9	62.8	0.7
Count Mixture	49.2	40.1	17.0	0.3
Semi-continuous Mixture	24.1	19.1	10.9	0.1

Table 1: Average effective samples per seconds (ESS/sec) for the coefficients β_0 and β_P from the simulation study. The rows pertain to the spatial two-part model used to generate the simulated observations. The columns denote the four methods implemented in the simulation study - PICAR-Z, correlated PICAR-Z, fixed rank kriging, and the ‘gold standard’ using reparameterization. The ESS/sec values are averaged over all 100 samples corresponding to a specific two-part model.

	PICAR-Z	Correlated PICAR-Z	Fixed Rank Kriging	Gold Standard
β_{1O}	0.94	0.94	0.83	0.94
β_{2O}	0.96	0.95	0.88	0.97
β_{1P}	0.75	0.74	0.86	0.86
β_{2P}	0.82	0.83	0.89	0.90

Table 2: Count Hurdle Case: Coverage probabilities for the coefficients β_0 and β_P from the simulation study. The rows pertain to the four regression coefficients - β_{1O} , β_{2O} , β_{1P} , and β_{2P} . The columns denote the four methods implemented in the simulation study - PICAR-Z, correlated PICAR-Z, fixed rank kriging, and the ‘gold standard’ using reparameterization. Coverage probabilities are computed using the 100 simulated samples.

3 Estimation of Cross-Correlation

In this section, we propose a modification of the PICAR-Z approach to model the cross-covariance between the occurrence $O(\mathbf{s})$ and prevalence processes $P(\mathbf{s})$. We extend the general modeling framework from Recta et al. (2012) to high-dimensional settings by imposing correlation on the dimension-reduced PICAR basis coefficients δ_o and δ_p .

Suppose we have realizations $\mathbf{W}_o = (W_o(\mathbf{s}_1), \dots, W_o(\mathbf{s}_1))'$ and $\mathbf{W}_p = (W_p(\mathbf{s}_1), \dots, W_p(\mathbf{s}_1))'$ from the occurrence and prevalence processes, respectively. Past studies (Recta et al., 2012; Oliver, 2003) have modeled cross-covariance between two spatial processes as:

$$\begin{bmatrix} \mathbf{W}_O \\ \mathbf{W}_P \end{bmatrix} | \tau_o, \sigma_p^2, \phi_o, \phi_p \sim \mathcal{N} \left(\begin{bmatrix} \mathbf{0} \\ \mathbf{0} \end{bmatrix}, \begin{bmatrix} \sigma_o^2 \mathbf{R}_{\phi_o} & \rho \Sigma_{op} \\ \rho \Sigma'_{op} & \sigma_p^2 \mathbf{R}_{\phi_p} \end{bmatrix} \right). \quad (6)$$

where \mathbf{W}_O and \mathbf{W}_p are realizations from a spatial occurrence and prevalence pro-

	PICAR-Z	Correlated PICAR-Z	Fixed Rank Kriging	Gold Standard
β_{1O}	0.92	0.93	0.82	0.94
β_{2O}	0.92	0.94	0.87	0.93
β_{1P}	0.88	0.87	0.91	0.75
β_{2P}	0.90	0.92	0.91	0.85

Table 3: Semi-continuous Hurdle Case: Coverage probabilities for the coefficients β_0 and β_P from the simulation study. The rows pertain to the four regression coefficients - β_{1O} , β_{2O} , β_{1P} , and β_{2P} . The columns denote the four methods implemented in the simulation study - PICAR-Z, correlated PICAR-Z, fixed rank kriging, and the ‘gold standard’ using reparameterization. Coverage probabilities are computed using the 100 simulated samples.

	PICAR-Z	Correlated PICAR-Z	Fixed Rank Kriging	Gold Standard
β_{1O}	0.89	0.87	0.84	0.90
β_{2O}	0.94	0.96	0.90	0.89
β_{1P}	0.72	0.71	0.63	0.88
β_{2P}	0.65	0.67	0.62	0.86

Table 4: Count Mixture Case: Coverage probabilities for the coefficients β_0 and β_P from the simulation study. The rows pertain to the four regression coefficients - β_{1O} , β_{2O} , β_{1P} , and β_{2P} . The columns denote the four methods implemented in the simulation study - PICAR-Z, correlated PICAR-Z, fixed rank kriging, and the ‘gold standard’ using reparameterization. Coverage probabilities are computed using the 100 simulated samples.

cesses. $\sigma_o^2 \mathbf{R}_{\phi_o}$ and $\sigma_p^2 \mathbf{R}_{\phi_p}$ are the spatial covariance matrices for the spatial occurrence and prevalence processes with marginal variance parameters σ_o^2 and σ_p^2 and range parameters ϕ_o and ϕ_p . In this study, we utilize the Matérn class of covariance functions with smoothness $\nu = 0.5$, which results in the exponential covariance function. Here, the (i, j) -th element of the covariance matrix is $\sigma_o^2 \mathbf{R}_{\phi_o ij} = \sigma_o^2 \exp\{-\|\mathbf{s}_i - \mathbf{s}_j\|/\phi_o\}$ and $\sigma_p^2 \mathbf{R}_{\phi_p ij} = \sigma_p^2 \exp\{-\|\mathbf{s}_i - \mathbf{s}_j\|/\phi_p\}$. We assume that the covariance is isotropic and stationary; hence, the covariance is merely a function of the Euclidean distance between the two locations. The cross-covariance function is constructed by setting $\rho \Sigma_{op} = \rho \mathbf{L}_o \mathbf{L}_p$ as in Oliver (2003) where ρ is the correlation between the occurrence and prevalence processes (at the same location) and \mathbf{L}_o and \mathbf{L}_p are the Choleski factors of $\sigma_o^2 \mathbf{R}_{\phi_o}$ and $\sigma_p^2 \mathbf{R}_{\phi_p}$, respectively. That is, $\sigma_o^2 \mathbf{R}_{\phi_o} = \sigma_o^2 \mathbf{L}_o \mathbf{L}_o'$ and $\sigma_p^2 \mathbf{R}_{\phi_p} = \sigma_p^2 \mathbf{L}_p \mathbf{L}_p'$.

	PICAR-Z	Correlated PICAR-Z	Fixed Rank Kriging	Gold Standard
β_{1O}	0.11	0.06	0.40	0.54
β_{2O}	0.12	0.09	0.32	0.53
β_{1P}	0.53	0.50	0.33	0.50
β_{2P}	0.52	0.49	0.43	0.41

Table 5: Semi-continuous Mixture Case: Coverage probabilities for the coefficients β_0 and β_P from the simulation study. The rows pertain to the four regression coefficients - β_{1O} , β_{2O} , β_{1P} , and β_{2P} . The columns denote the four methods implemented in the simulation study - PICAR-Z, correlated PICAR-Z, fixed rank kriging, and the ‘gold standard’ using reparameterization. Coverage probabilities are computed using the 100 simulated samples.

Though this modeling framework has been successfully applied to Recta et al. (2012) to smaller datasets, it may be computationally prohibitive for larger datasets. For a sample of $n = 400$ observations, inference required 60 hours to generate 100,000 iterations of the Langevin-Hastings algorithm on a 3.0-GHz quadcore Intel Xeon processor with 32 GB of memory (Recta et al., 2012).

Instead, we propose modeling the cross-correlation among the PICAR-Z basis coefficients δ_o and δ_p , which results in cross-correlation between the resulting spatial random effects $\tilde{\mathbf{W}}_o \approx \Phi_o \delta_o$ and $\tilde{\mathbf{W}}_p \approx \Phi_p \delta_p$ for the occurrence and prevalence processes, respectively.

Suppose the matrices $\Phi_P \Phi_P'$ and $\Phi_O \Phi_O'$ are positive definite. If

$$\begin{bmatrix} \delta_O \\ \delta_P \end{bmatrix} \sim \mathcal{N} \left(\begin{bmatrix} \mathbf{0} \\ \mathbf{0} \end{bmatrix}, \begin{bmatrix} \tau_p^{-1} I & \rho \Sigma_{OP} \\ \rho \Sigma'_{OP} & \tau_p^{-1} I \end{bmatrix} \right)$$

where ρ is a correlation coefficient and $\Sigma_{OP} = \tau_o^{-1/2} \tau_p^{-1/2} \Phi_O' (\Phi_O \Phi_O')^{-1} L_1 L_2 (\Phi_P \Phi_P')^{-1} \Phi_P'$, then

$$\begin{bmatrix} \tilde{\mathbf{W}}_O \\ \tilde{\mathbf{W}}_P \end{bmatrix} \sim \mathcal{N} \left(\begin{bmatrix} \mathbf{0} \\ \mathbf{0} \end{bmatrix}, \begin{bmatrix} \tau_o^{-1/2} \Phi_O \Phi_O' & \rho L_O L_P' \\ \rho L_P L_O' & \tau_p^{-1/2} \Phi_P \Phi_P' \end{bmatrix} \right).$$

From this, we can model the cross-covariance between the occurrence $O(\mathbf{s})$ and preva-

lence $P(\mathbf{s})$ spatial processes by inferring the cross-correlation between the basis coefficients $\boldsymbol{\delta}_o$ and $\boldsymbol{\delta}_p$. Under the PICAR-Z modeling framework, the dimensions of $\boldsymbol{\delta}_o$ and $\boldsymbol{\delta}_p$ are much smaller than n . By inferring the cross-correlation between $\boldsymbol{\delta}_o$ and $\boldsymbol{\delta}_p$, we are able to bypass the expensive matrix operations (e.g determinants and inverses) typically associated with the cross-covariance model in Equation 6.

We modify the PICAR-Z hierarchical two-part modeling framework to account for cross-correlation:

$$\begin{aligned}
\text{Data Model:} & \quad Z(\mathbf{s})|O(\mathbf{s}), P(\mathbf{s}) \sim F(\cdot | O(\mathbf{s}), P(\mathbf{s})) \\
\text{Process Model:} & \quad O(\mathbf{s})|\pi(\mathbf{s}) \sim \text{Bern}(\pi(\mathbf{s})) \\
& \quad P(\mathbf{s})|\boldsymbol{\theta}(\mathbf{s}) \sim \tilde{F}(\cdot|\boldsymbol{\theta}(\mathbf{s})) \\
\text{Sub-process Model 1:} & \quad \pi(\mathbf{s})|\eta_o(\mathbf{s}) = g_o^{-1}(\eta_o(\mathbf{s})) \\
\text{(Occurrence)} & \quad \eta_o(\mathbf{s})|\boldsymbol{\beta}_o, \boldsymbol{\delta}_o(\mathbf{s}) = \mathbf{X}(\mathbf{s})'\boldsymbol{\beta}_o + [\mathbf{A}_o\mathbf{M}_o\boldsymbol{\delta}_o](\mathbf{s}) \\
\text{Sub-process Model 2:} & \quad \theta(\mathbf{s})|\eta_p(\mathbf{s}) = g_p^{-1}(\eta_p(\mathbf{s})) \\
\text{(Prevalence)} & \quad \eta_p(\mathbf{s})|\boldsymbol{\beta}_p, \boldsymbol{\delta}_p(\mathbf{s}) = \mathbf{X}(\mathbf{s})'\boldsymbol{\beta}_p + [\mathbf{A}_p\mathbf{M}_p\boldsymbol{\delta}_p](\mathbf{s}) \\
& \quad \begin{bmatrix} \boldsymbol{\delta}_O \\ \boldsymbol{\delta}_P \end{bmatrix} | \tau_o, \tau_p, \rho \sim \mathcal{N} \left(\begin{bmatrix} \mathbf{0} \\ \mathbf{0} \end{bmatrix}, \begin{bmatrix} \tau_o^{-1}I & \rho\Sigma_{OP} \\ \rho\Sigma'_{OP} & \tau_p^{-1}I \end{bmatrix} \right) \\
\text{Parameter Model:} & \quad \boldsymbol{\beta}_o \sim \mathcal{N}(\boldsymbol{\mu}_{\beta_o}, \Sigma_{\beta_o}), \quad \boldsymbol{\beta}_p \sim \mathcal{N}(\boldsymbol{\mu}_{\beta_p}, \Sigma_{\beta_p}) \\
& \quad \tau_o \sim \mathcal{G}(\alpha_{\tau_o}, \beta_{\tau_o}), \quad \tau_p \sim \mathcal{G}(\alpha_{\tau_p}, \beta_{\tau_p})
\end{aligned}$$

where $F(\cdot | O(\mathbf{s}), P(\mathbf{s}))$ is the distribution of the specified two-part model, and $\tilde{F}(\cdot|\boldsymbol{\theta}(\mathbf{s}))$ denotes the distribution function of the prevalence process. \mathbf{A}_o and \mathbf{A}_p are the projectors matrices for the occurrence and prevalence processes, respectively. For the occurrence and prevalence processes, respectively, the Moran's basis functions matrices are \mathbf{M}_o and \mathbf{M}_p , the basis coefficients are $\boldsymbol{\delta}_o$ and $\boldsymbol{\delta}_p$, and the precision parameters are τ_o and τ_p . The cross-correlation coefficient is ρ with cross-covariance matrix $\Sigma_{OP} =$

$\tau_o^{-1/2} \tau_p^{-1/2} \Phi'_O (\Phi_O \Phi'_O)^{-1} L_1 L_2 (\Phi_P \Phi'_P)^{-1} \Phi'_P$. Similar to the PICAR-Z framework (with no cross-covariance), \mathbf{Q} is typically fixed prior to model fitting (see Lee and Haran (2021) for additional details).

4 Applications

		$\hat{\beta}_1$ (95% CI) Median grain size	$\hat{\beta}_2$ (95% CI) Silt content	$\hat{\beta}_3$ (95% CI) Altitude
Count Hurdle	PICAR-Z	-0.071 (-0.265 , 0.131)	0.138 (-0.028 , 0.305)	0.554 (0.459 , 0.644)
	PICAR-Z (Cor)	-0.093 (-0.297 , 0.102)	0.131 (-0.033 , 0.303)	0.557 (0.461 , 0.647)
	Bi-square	-0.163 (-0.396 , 0.066)	-0.034 (-0.229 , 0.153)	0.49 (0.385 , 0.595)
Count Mixture	PICAR-Z	-0.126 (-0.361 , 0.129)	0.009 (-0.194 , 0.207)	0.491 (0.38 , 0.604)
	PICAR-Z (Cor)	-0.138 (-0.374 , 0.109)	0.008 (-0.185 , 0.207)	0.497 (0.389 , 0.606)
	Bi-square	-0.242 (-0.54 , 0.046)	-0.239 (-0.475 , 0.005)	0.447 (0.32 , 0.577)

Table 6: Parameter estimation for the bi-valve species count data example (Occurrence). Columns correspond to the parameter estimates and 95% credible intervals for the regression coefficients corresponding to the three covariates (mean grain size, silt content, and altitude) for the occurrence process. Rows denote the model-fitting approach.

		$\hat{\beta}_1$ (95% CI) Median grain size	$\hat{\beta}_2$ (95% CI) Silt content	$\hat{\beta}_3$ (95% CI) Altitude
Count Hurdle	PICAR-Z	0.126 (0.024 , 0.227)	0.46 (0.38 , 0.546)	0.229 (0.18 , 0.279)
	PICAR-Z (Cor)	0.137 (0.027 , 0.235)	0.467 (0.382 , 0.547)	0.228 (0.178 , 0.278)
	Bi.square	0.11 (0.009 , 0.218)	0.505 (0.421 , 0.589)	0.24 (0.187 , 0.293)
Count Mixture	PICAR-Z	0.11 (0.013 , 0.212)	0.435 (0.357 , 0.513)	0.214 (0.161 , 0.261)
	PICAR-Z (Cor)	0.113 (0.013 , 0.21)	0.438 (0.353 , 0.52)	0.212 (0.163 , 0.263)
	Bi-square	0.111 (0.009 , 0.206)	0.509 (0.428 , 0.589)	0.247 (0.196 , 0.298)

Table 7: Parameter estimation for the bi-valve species count data example (Prevalence). Columns correspond to the parameter estimates and 95% credible intervals for the regression coefficients corresponding to the three covariates (mean grain size, silt content, and altitude) for the prevalence process. Rows denote the model-fitting approach.

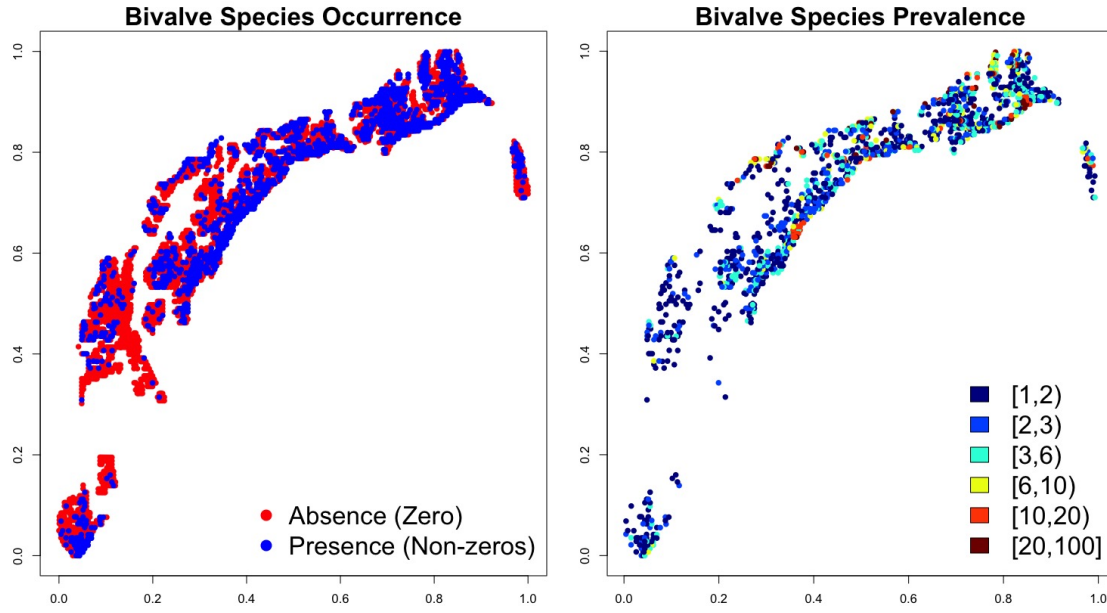


Figure 1: Maps of occurrence (left) and prevalence (right) of the Baltic tellin (*Macoma balthica*) species. For the occurrence map, the blue points denote the presence and the red points denote absence of the bivalve species. The prevalence map displays counts at the locations with positive counts.

References

- Agarwal, D. K., Gelfand, A. E., and Citron-Pousty, S. (2002). Zero-inflated models with application to spatial count data. *Environmental and Ecological Statistics*, 9(4):341–355.
- Arcuti, S., Pollice, A., Ribecco, N., and D’Onghia, G. (2016). Bayesian spatiotemporal analysis of zero-inflated biological population density data by a delta-normal spatiotemporal additive model: Bayesian analysis of zero-inflated biological data. *Biometrical Journal*, 58(2):372–386.
- Banerjee, A., Dunson, D. B., and Tokdar, S. T. (2013). Efficient Gaussian process regression for large datasets. *Biometrika*, 100(1):75–89.
- Banerjee, S., Gelfand, A. E., Finley, A. O., and Sang, H. (2008). Gaussian predictive process models for large spatial data sets. *Journal of the Royal Statistical Society: Series B (Statistical Methodology)*, 70(4):825–848.

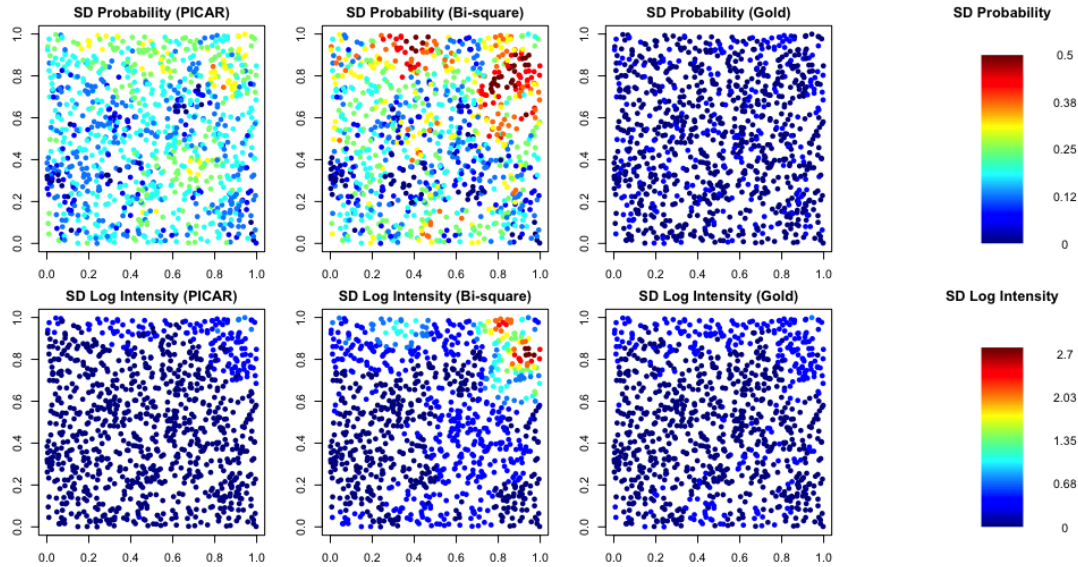


Figure 2: Prediction uncertainty for a single simulated example. Data are generated from the spatial count mixture model in the simulation study. Top row includes the standard deviation of the predicted probability surface $\pi(\mathbf{s})$ for the occurrence random process $O(\mathbf{s})$. Bottom row presents the log-intensity surface $\log(\theta(\mathbf{s}))$ for the prevalence random process $P(\mathbf{s})$. Column 1 presents the true latent probability and log-intensity surfaces. Columns 2-3 include the predicted surfaces for PICAR-Z (column 2), fixed rank kriging with bisquare basis functions (column 3), and the ‘gold standard’ approach (column 4). In the fifth column, a color scale is provided for the probability and log-intensity surfaces.

Bijleveld, A. I., van Gils, J. A., van der Meer, J., Dekinga, A., Kraan, C., van der Veer, H. W., and Piersma, T. (2012). Designing a benthic monitoring programme with multiple conflicting objectives. *Methods in Ecology and Evolution*, 3(3):526–536.

Bopp, G. P., Shaby, B. A., Forest, C. E., and Mejía, A. (2020). Projecting flood-inducing precipitation with a Bayesian analogue model. *Journal of Agricultural, Biological and Environmental Statistics*, 25(2):229–249.

Bradley, J. R., Holan, S. H., and Wikle, C. K. (2019). Bayesian hierarchical models with conjugate full-conditional distributions for dependent data from the natural exponential family. *Journal of the American Statistical Association*, 0(ja):1–29.

Bradley, J. R., Wikle, C. K., and Holan, S. H. (2015). Spatio-temporal change of support

- with application to American Community Survey multi-year period estimates. *Stat*, 4(1):255–270.
- Brenner, S. and Scott, R. (2007). *The Mathematical Theory of Finite Element Methods*, volume 15. Springer Science & Business Media.
- Chai, H. S. and Bailey, K. R. (2008). Use of log-skew-normal distribution in analysis of continuous data with a discrete component at zero. *Statistics in medicine*, 27(18):3643–3655.
- Chang, W., Haran, M., Applegate, P., and Pollard, D. (2016). Calibrating an ice sheet model using high-dimensional binary spatial data. *Journal of the American Statistical Association*, 111(513):57–72.
- Christensen, O. F., Roberts, G. O., and Sköld, M. (2006). Robust Markov chain Monte Carlo methods for spatial generalized linear mixed models. *Journal of Computational and Graphical Statistics*, 15(1):1–17.
- Christensen, O. F. and Waagepetersen, R. (2002). Bayesian prediction of spatial count data using generalized linear mixed models. *Biometrics*, 58(2):280–286.
- Compton, T. J., Holthuijsen, S., Koolhaas, A., Dekinga, A., ten Horn, J., Smith, J., Galama, Y., Brugge, M., van der Wal, D., van der Meer, J., et al. (2013). Distinctly variable mudscapes: Distribution gradients of intertidal macrofauna across the dutch wadden sea. *Journal of Sea Research*, 82:103–116.
- Cressie, N. and Johannesson, G. (2008). Fixed rank kriging for very large spatial data sets. *Journal of the Royal Statistical Society: Series B (Statistical Methodology)*, 70(1):209–226.
- Cressie, N. and Wikle, C. K. (2015). *Statistics for spatio-temporal data*. John Wiley & Sons.

- de Valpine, P., Turek, D., Paciorek, C., Anderson-Bergman, C., Temple Lang, D., and Bodik, R. (2017). Programming with models: writing statistical algorithms for general model structures with nimble. *Journal of Computational and Graphical Statistics*, 26:403–413.
- Deschamps, P., Durand, N., Bard, E., Hamelin, B., Camoin, G., Thomas, A. L., Henderson, G. M., Okuno, J., and Yokoyama, Y. (2012). Ice-sheet collapse and sea-level rise at the Bølling warming 14,600 years ago. *Nature*, 483(7391):559.
- Diggle, P. J., Tawn, J. A., and Moyeed, R. (1998). Model-based geostatistics. *Journal of the Royal Statistical Society: Series C (Applied Statistics)*, 47(3):299–350.
- Dreassi, E., Petrucci, A., and Rocco, E. (2014). Small area estimation for semicontinuous skewed spatial data: An application to the grape wine production in tuscany. *Biometrical Journal*, 56(1):141–156.
- Feng, C. X. (2021). A comparison of zero-inflated and hurdle models for modeling zero-inflated count data. *Journal of Statistical Distributions and Applications*, 8(1):1–19.
- Fernandes, M. V., Schmidt, A. M., and Migon, H. S. (2009). Modelling zero-inflated spatio-temporal processes. *Statistical Modelling: An International Journal*, 9(1):3–25.
- Fretwell, P., Pritchard, H., Vaughan, D., Bamber, J., Barrand, N., Bell, R., Bianchi, C., Bingham, R., Blankenship, D., Casassa, G., et al. (2012). Bedmap2: Improved ice bed, surface and thickness datasets for Antarctica. *The Cryosphere Discussions*, 6:4305–4361.
- Fruhworth-Schnatter, S. and Pyne, S. (2010). Bayesian inference for finite mixtures of univariate and multivariate skew-normal and skew-t distributions. *Biostatistics*, 11(2):317–336.
- Griffith, D. A. (2003). Spatial filtering. In *Spatial Autocorrelation and Spatial Filtering*, pages 91–130. Springer.

- Gschlößl, S. and Czado, C. (2008). Modelling count data with overdispersion and spatial effects. *Statistical Papers*, 49(3):531–552.
- Guan, Y. and Haran, M. (2018). A computationally efficient projection-based approach for spatial generalized linear mixed models. *Journal of Computational and Graphical Statistics*, 27(4):701–714.
- Guan, Y. and Haran, M. (2019). Fast expectation-maximization algorithms for spatial generalized linear mixed models. *arXiv preprint arXiv:1909.05440*.
- Guhaniyogi, R., Finley, A. O., Banerjee, S., and Gelfand, A. E. (2011). Adaptive Gaussian predictive process models for large spatial datasets. *Environmetrics*, 22(8):997–1007.
- Haran, M. (2011). Gaussian random field models for spatial data. *Handbook of Markov Chain Monte Carlo*, pages 449–478.
- Haran, M., Hodges, J. S., and Carlin, B. P. (2003). Accelerating computation in markov random field models for spatial data via structured MCMC. *Journal of Computational and Graphical Statistics*, 12(2):249–264.
- Higdon, D. (1998). A process-convolution approach to modelling temperatures in the North Atlantic Ocean. *Environmental and Ecological Statistics*, 5(2):173–190.
- Hjelle, Ø. and Dæhlen, M. (2006). *Triangulations and applications*. Springer Science & Business Media.
- Hughes, J. and Haran, M. (2013). Dimension reduction and alleviation of confounding for spatial generalized linear mixed models. *Journal of the Royal Statistical Society: Series B (Statistical Methodology)*, 75(1):139–159.
- Katzfuss, M. (2017). A multi-resolution approximation for massive spatial datasets. *Journal of the American Statistical Association*, 112(517):201–214.

- Kim, S. H., Chang, C.-C. H., Kim, K. H., Fine, M. J., and Stone, R. A. (2012). BLUP (REMQ) estimation of a correlated random effects negative binomial hurdle model. *Health Services and Outcomes Research Methodology*, 12(4):302–319.
- Kleiber, W. and Nychka, D. (2012). Nonstationary modeling for multivariate spatial processes. *Journal of Multivariate Analysis*, 112:76–91.
- Krock, M., Kleiber, W., Hammerling, D., and Becker, S. (2021). Modeling massive highly-multivariate nonstationary spatial data with the basis graphical lasso. *arXiv preprint arXiv:2101.02404*.
- Lambert, D. (1992). Zero-inflated Poisson regression, with an application to defects in manufacturing. *Technometrics*, 34(1):1–14.
- Lee, B. S. and Haran, M. (2021). PICAR: an efficient extendable approach for fitting hierarchical spatial models. *Technometrics*, pages 1–12.
- Lee, C.-E. and Kim, S. (2017). Applicability of zero-inflated models to fit the torrential rainfall count data with extra zeros in south korea. *Water*, 9(2):123.
- Lee, Y., Alam, M. M., Noh, M., Rönnegård, L., and Skarin, A. (2016). Spatial modeling of data with excessive zeros applied to reindeer pellet-group counts. *Ecology and evolution*, 6(19):7047–7056.
- Lehoucq, R. B., Sorensen, D. C., and Yang, C. (1998). *ARPACK users' guide: Solution of large-scale eigenvalue problems with implicitly restarted Arnoldi methods*, volume 6. Siam.
- Lindgren, F., Rue, H., et al. (2015). Bayesian spatial modelling with R-INLA. *Journal of Statistical Software*, 63(19):1–25.
- Lindgren, F., Rue, H., and Lindström, J. (2011). An explicit link between Gaussian fields and Gaussian Markov random fields: the stochastic partial differential equation

- approach. *Journal of the Royal Statistical Society: Series B (Statistical Methodology)*, 73(4):423–498.
- Liu, L., Strawderman, R. L., Johnson, B. A., and O’Quigley, J. M. (2016). Analyzing repeated measures semi-continuous data, with application to an alcohol dependence study. *Statistical Methods in Medical Research*, 25(1):133–152.
- Lyashevskaya, O., Brus, D. J., and van der Meer, J. (2016). Mapping species abundance by a spatial zero-inflated Poisson model: A case study in the Wadden Sea, the Netherlands. *Ecology and Evolution*, 6(2):532–543.
- McGranahan, G., Balk, D., and Anderson, B. (2007). The rising tide: Assessing the risks of climate change and human settlements in low elevation coastal zones. *Environment and Urbanization*, 19(1):17–37.
- Min, Y. and Agresti, A. (2005). Random effect models for repeated measures of zero-inflated count data. *Statistical modelling*, 5(1):1–19.
- Moran, P. A. (1950). Notes on continuous stochastic phenomena. *Biometrika*, 37(1/2):17–23.
- Moulton, L. H. and Halsey, N. A. (1995). A mixture model with detection limits for regression analyses of antibody response to vaccine. *Biometrics*, pages 1570–1578.
- Mullahy, J. (1986). Specification and testing of some modified count data models. *Journal of Econometrics*, 33(3):341–365.
- Neelon, B. (2019). Bayesian zero-inflated negative binomial regression based on Pólya-gamma mixtures. *Bayesian Analysis*, 14(3):829.
- Neelon, B., Chang, H. H., Ling, Q., and Hastings, N. S. (2016a). Spatiotemporal hurdle models for zero-inflated count data: Exploring trends in emergency department visits. *Statistical Methods in Medical Research*, 25(6):2558–2576.

- Neelon, B., O'Malley, A. J., and Smith, V. A. (2016b). Modeling zero-modified count and semicontinuous data in health services research Part 1: Background and overview. *Statistics in Medicine*, 35(27):5070–5093.
- Neelon, B., O'Malley, A. J., and Normand, S.-L. T. (2011). A Bayesian two-part latent class model for longitudinal medical expenditure data: Assessing the impact of mental health and substance abuse parity. *Biometrics*, 67(1):280–289.
- Neelon, B., Zhu, L., and Neelon, S. E. B. (2015). Bayesian two-part spatial models for semicontinuous data with application to emergency department expenditures. *Biostatistics*, 16(3):465–479.
- Nicholls, R. J., Tol, R. S., and Vafeidis, A. T. (2008). Global estimates of the impact of a collapse of the West Antarctic ice sheet: An application of FUND. *Climatic Change*, 91(1-2):171.
- Nychka, D., Bandyopadhyay, S., Hammerling, D., Lindgren, F., and Sain, S. (2015). A multiresolution Gaussian process model for the analysis of large spatial datasets. *Journal of Computational and Graphical Statistics*, 24(2):579–599.
- Oliver, D. S. (2003). Gaussian cosimulation: modelling of the cross-covariance. *Mathematical Geology*, 35(6):681–698.
- Olsen, M. K. and Schafer, J. L. (2001). A two-part random-effects model for semicontinuous longitudinal data. *Journal of the American Statistical Association*, 96(454):730–745.
- Park, J. and Haran, M. (2020). Reduced-dimensional Monte Carlo maximum likelihood for latent Gaussian random field models. *Journal of Computational and Graphical Statistics*, 30(2):269–283.
- Qiu, Y. and Mei, J. (2019). *RSpectra: Solvers for Large-Scale Eigenvalue and SVD Problems*. R package version 0.15-0.

- Rasmussen, C. and Williams, C. (2006). *Gaussian Processes for Machine Learning*. Adaptive Computation and Machine Learning. MIT Press, Cambridge, MA, USA.
- Rasmussen, C. E. (2004). Gaussian processes in machine learning. In *Advanced Lectures on Machine Learning*, pages 63–71. Springer.
- Rathbun, S. L. and Fei, S. (2006). A spatial zero-inflated poisson regression model for oak regeneration. *Environmental and Ecological Statistics*, 13(4):409–426.
- Recta, V., Haran, M., and Rosenberger, J. L. (2012). A two-stage model for incidence and prevalence in point-level spatial count data. *Environmetrics*, 23(2):162–174.
- Roeder, K., Lynch, K. G., and Nagin, D. S. (1999). Modeling uncertainty in latent class membership: A case study in criminology. *Journal of the American Statistical Association*, 94(447):766–776.
- Rue, H., Martino, S., and Chopin, N. (2009). Approximate Bayesian inference for latent Gaussian models by using integrated nested Laplace approximations. *Journal of the Royal Statistical Society: Series B (Statistical Methodology)*, 71(2):319–392.
- Sengupta, A. and Cressie, N. (2013). Hierarchical statistical modeling of big spatial datasets using the exponential family of distributions. *Spatial Statistics*, 4:14–44.
- Stein, M. L. (2012). *Interpolation of Spatial Data: Some Theory for Kriging*. Springer Science & Business Media.
- Tobin, J. (1958). Estimation of relationships for limited dependent variables. *Econometrica: Journal of the Econometric Society*, pages 24–36.
- Ver Hoef, J. M. and Jansen, J. K. (2007). Space—time zero-inflated count models of harbor seals. *Environmetrics*, 18(7):697–712.
- Vuong, Q. H. (1989). Likelihood ratio tests for model selection and non-nested hypotheses. *Econometrica: Journal of the Econometric Society*, pages 307–333.

Wang, X., Chen, M.-H., Kuo, R. C., and Dey, D. K. (2015). Bayesian spatial-temporal modeling of ecological zero-inflated count data. *Statistica Sinica*, 25(1):189.